Molecular Therapy
Original Article

The Circular RNA Interacts with STAT3, Increasing Its Nuclear Translocation and Wound Repair by Modulating Dnmt3a and miR-17 Function

Zhen-Guo Yang,[1,2,3,7,8] Faryal Mehwish Awan,[1,3,4,7] William W. Du,[1,3,7] Yan Zeng,[1,3,5,7] Juanjuan Lyu,[1,3] De Wu,[2] Shaan Gupta,[1,3] Weining Yang,[6] and Burton B. Yang[1,3,6]

[1]Sunnybrook Research Institute, Sunnybrook Health Sciences Centre, Toronto, ON M4N 3M5, Canada; [2]Institute of Animal Nutrition, Sichuan Agricultural University, 211 Huimin Road, Wenjiang District, Chengdu, 611130 Sichuan, China; [3]Department of Laboratory Medicine and Pathobiology, University of Toronto, Toronto, ON M5S 1A8, Canada; [4]Atta-ur-Rahman School of Applied Biosciences (ASAB), National University of Sciences and Technology (NUST), H-12 Islamabad, Pakistan; [5]Department of Cardiovascular Medicine, Second Xiangya Hospital of Central South University, 139 Middle Ren-Min Road, Changsha, 410011 Hunan, China; [6]Institute of Medical Science, University of Toronto, Toronto, ON M5S 1A8, Canada

Delayed or impaired wound healing is a major health issue worldwide, especially in patients with diabetes and atherosclerosis. Here we show that expression of the circular RNA circ-Amotl1 accelerated healing process in a mouse excisional wound model. Further studies showed that ectopic circ-Amotl1 increased protein levels of Stat3 and Dnmt3a. The increased Dnmt3a then methylated the promoter of microRNA miR-17, decreasing miR-17-5p levels but increasing fibronectin expression. We found that Stat3, similar to Dnmt3a and fibronectin, was a target of miR-17-5p. Decreased miR-17-5p levels would increase expression of fibronectin, Dnmt3a, and Stat3. All of these led to increased cell adhesion, migration, proliferation, survival, and wound repair. Furthermore, we found that circ-Amotl1 not only increased Stat3 expression but also facilitated Stat3 nuclear translocation. Thus, the ectopic expressed circ-Amotl1 and Stat3 were mainly translocated to nucleus. In the presence of circ-Amotl1, Stat3 interacted with Dnmt3a promoter with increased affinity, facilitating Dnmt3a transcription. Ectopic application of circ-Amotl1 accelerating wound repair may shed light on skin wound healing clinically.

INTRODUCTION

As the largest organ of human body, the skin acts as the first line of protection against environmental hazards. Dysfunctions of the skin's wound-healing process can result in cosmetic problems, metabolic disorders, and lethal infection. Cutaneous wound healing is a complex biological process that consists of hemostasis, inflammation, re-epithelization, vascularization, and tissue remolding. Delayed or impaired wound healing has been a major public health issue worldwide, especially in patients with diabetes mellitus and vascular atherosclerosis. We recently found that a newly detected class of genetic material circular RNAs (circRNAs) may be crucial in tissue remodeling, because the circRNA circ-Foxo3 plays roles in regulating cell cycle progression, cell senescence, cardiovascular protection, and tumor formation.[1–4] Recent studies have shown that a wide array of endogenous circRNAs are expressed in animal cells, while certain circRNAs are highly specific to cell type and/or developmental stage, suggesting potential roles in developmental regulation.[5–9] Genome-wide analyses have revealed high levels of abundance and evolutionary conservation of circRNAs across species, suggesting specific roles in cellular physiology.[9–12]

One mode of action found on some circRNAs is the sponging activity of this class of molecules to bind miRNAs, allowing them to arrest miRNA activity.[13–15] The circRNA CiRS-7 or CDR1as, which is highly expressed in neuronal tissues, possesses many microRNA (miRNA)-binding sites and has been shown to sponge miRNA functions.[7] The circRNA SRY, which is highly expressed in murine testes, functions as miR-138 sponge.[7,16] We have recently found that circ-Foxo3, along with the pseudogene of Foxo3, can sponge a number of miRNAs and repress breast cancer development.[1] In the present report, we show that the circRNA circ-Amotl1 can accelerate wound healing by binding to Stat3. circ-Amotl1 then facilitated Stat3 nuclear translocation and binding to Dnmt3a promoter, which enhanced Dnmt3a expression and modulated miR-17 function.

RESULTS

Enhanced Wound Healing in Mice Delivered with circ-Amotl1

In this study, we explored the potential involvement of circ-Amotl1 in wound repair. C57BL/6xCBA mice were subject to a cervical dermal punch biopsy, which left full-thickness excisional wounds of about 5 mm on both sides of the back. The next day, the wound areas were injected with circ-Amotl1 expression plasmids (Figure S1A) or

Received 14 January 2017; accepted 31 May 2017;
http://dx.doi.org/10.1016/j.ymthe.2017.05.022.

[7]These authors contributed equally to this work.

[8]Present address: College of Animal Science and Technology, Southwest University, Chongqing 400715, China

Correspondence: Burton B. Yang, S110, S-Wing Research Building, Sunnybrook Health Sciences Centre, 2075 Bayview Avenue, Toronto, ON M4N 3M5, Canada.
E-mail: byang@sri.utoronto.ca

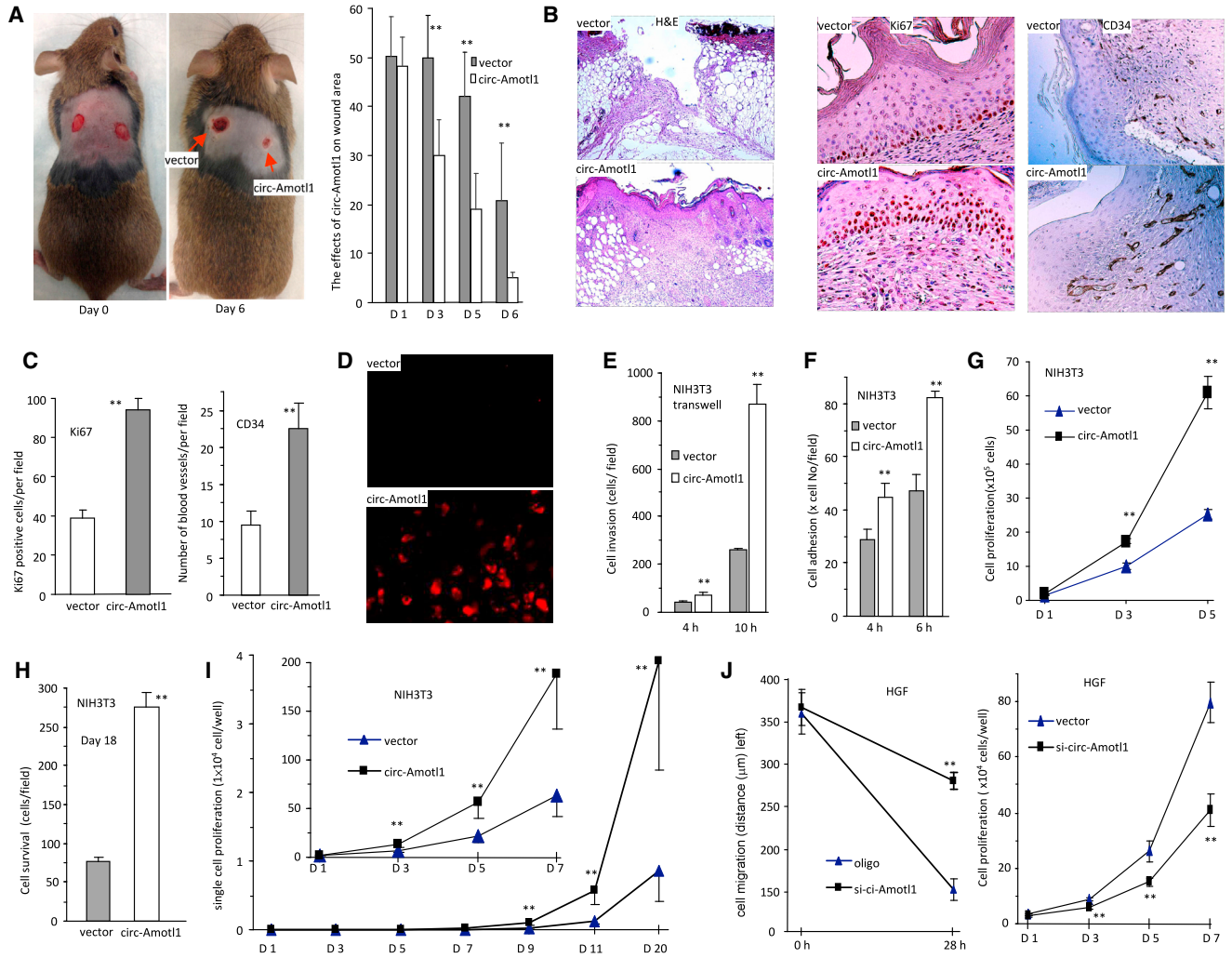

Figure 1. circ-Amotl1 Enhanced Wound Healing, Proliferation, and Migration

(A) Left: wild-type mice were subjected to wound healing assay (n = 10). Pictures were taken from the sixth day after wounding, showing that injection with circ-Amotl1 plasmids enhanced wound healing. Right: graph representing wound sizes during the 6-day healing process, which were measured by multiplying longest length by greatest width (n = 10). (B) Sections of wound tissues from circ-Amotl1- and vector-injected mice were subjected to H&E staining (left) and immunostaining for Ki67 and CD34 expression (right). (C) The numbers of Ki67-positive cells and stained blood vessels were counted and quantified. circ-Amotl1 injection enhanced Ki67 and CD34 expression in the wound tissues (n = 5). (D) In situ hybridization showing expression of circ-Amotl1 in the wound tissues. (E) Transwell migration assay showed that more circ-Amotl1-transfected cells migrated through the membrane than control groups after 4 and 10 hr (n = 5). (F) The cells were incubated in a Petri dish for 4 or 6 hr. More circ-Amotl1-transfected cells adhered to the plates than control (n = 5). (G) Cell proliferation was assayed. Cells transfected with circ-Amotl1 displayed increased proliferation compared with control (n = 5). (H) The cells were maintained in serum-free medium for survival assay. circ-Amotl1 expression increased survival rates after 18 days (n = 5). (I) In single-cell culturing assay, the number of cells per well was counted as indicated for up to 20 days. Cells transfected with circ-Amotl1 displayed increased cell proliferation compared with control (n = 20). (J) Left: wound-healing assay showed that silencing circ-Amotl1 decreased cell migration in HGF cells transfected with circ-Amotl1 siRNA. Right: silencing circ-Amotl1 repressed cell proliferation in HGF cells transfected with siRNA. **p < 0.01. Error bars denote SD (n = 5).

a control vector at a volume of 100 μL, containing 50 μg plasmids per site. The injection was repeated every other day. The sizes of the wound areas were measured every other day. Six days after wounding, the wounds injected with circ-Amotl1 expression plasmids showed enhanced healing compared with the wounds injected with the vector (Figure 1A, left). Studies have shown that genders and sex steroids might affect tissue repair and regeneration.[17] In our studies, both male and female mice injected with circ-Amotl1 displayed accelerated wound healing. The difference in wound area between two groups was statistically significant after 6 days (Figure 1A, right). Measurements of wound area revealed that the ratios of unhealed space (day 6/day 1) were significantly smaller in the group injected with circ-Amotl1 than that in the control (Figure S1B).

On the seventh day, tissues of the wound were biopsied for histological examination and immunohistochemistry staining. Wound healing is

driven by proliferation and migration of cells in the wound, including fibroblasts and myofibroblasts. H&E staining showed that there was increased cell density in the wounds injected with circ-Amotl1, compared with the control wounds (Figure 1B, left). We also found that there were more new blood vessels and Ki67-positive cells generated in the wounds injected with circ-Amotl1, as evaluated by CD34 levels (Figure 1B, right). Quantitation of the numbers of stained blood vessels and Ki67-positive cells showed significant increases in the circ-Amotl1-injected mice (Figure 1C). We confirmed that the circ-Amotl1 plasmids were expressed in the wound by in situ hybridization using a probe specifically recognizing circ-Amolt1 (Figure 1D).

circ-Amotl1 Expression Accelerates Fibroblast Proliferation and Migration

Fibroblasts are known to play essential roles in tissue repair. They move to wound areas upon wound formation and synthesize collagen and fibronectin together with other extracellular matrix (ECM) molecules, generating the force required to contract the wound. To study the function of circ-Amotl1 on fibroblast activities, NIH 3T3 fibroblasts were stably transfected with the plasmids. Real-time PCR was used to confirm the expression of circ-Amotl1 in the transfected cells. There was a significant elevation of circ-Amotl1 in cells transfected with circ-Amotl1 expression plasmids (Figure S1C).

We performed a number of cell activity assays to test the effects of circ-Amotl1 on cell biology associated with wound repair. In cell migration assay, the circ-Amotl1-transfected cells showed a greater ability to migrate compared with the vector-transfected cells (Figure S1D). The locomotion of fibroblasts during wound healing includes migration as well as deformation. Thus, transwell migration assay was performed to test both functions. After being placed above a cell-permeable membrane for 10 hr, more circ-Amotl1-transfected cells migrated through microspores of the membrane (Figures 1E and S1E). In cell adhesion assay, NIH 3T3 cells were incubated in a Petri dish for 4–6 hr. It was found that more circ-Amotl1-transfected cells were able to attach to the surface of the Petri dish (Figure 1F). In proliferation and survival assays, we found that circ-Amotl1 expression increased cell proliferation (Figure 1G) and survival (Figure 1H). We examined the effect of circ-Amolt1 on each cell by performing single-cell culture assay and found that circ-Amotl1 expression greatly promoted cell proliferation (Figure 1I).

The effect of circ-Amotl1 was also performed in the human gingival fibroblast (HGF; named CRL-2014, from ATCC) cell line, which allowed us to obtain stably transfected cell lines and could be maintained for long-term experiments for mechanistic studies. After confirming upregulation of circ-Amotl1 (Figure S2A), we detected increased cell migration (Figure S2B), adhesion (Figure S2C), proliferation (Figure S2D), and survival (Figure S2E). We examined the effect of endogenous circ-Amotl1 by silencing circ-Amotl1 using a small interfering RNA (siRNA) approach (Figure S2F). Silencing endogenous circ-Amotl1 decreased HGF cell migration and proliferation (Figure 1J). It also decreased cell adhesion (Figure S2G) and survival (Figure S2H).

Interaction of circ-Amotl1 with Stat3

Because circ-Amotl1 greatly promoted cell proliferation, we anticipated that circ-Amotl1 might interact with mitosis-associated proteins. Cell lysis prepared from NIH 3T3 cells were subject to immunoprecipitation for pre-screening with anti-rabbit IgG, mouse IgG, E2F1, E2F5, E2F4, EGF, ETS-1, HIF-1a, AP1, NF1, Stat1, Sox2, Par4, Stat3, ID1, Erk, and Ago2 antibodies, followed by real-time PCR with primers specific for the linear Amotl1 mRNA or circ-Amotl1. The experiment showed that circ-Amotl1 was pulled down by immunoprecipitation experiments with antibodies against E2F1, E2F4, EGF, ETS-1, AP1, NF1, and Stat3, which did not pull down linear Amotl1 mRNA (Figure 2A). The anti-Stat3 antibody pulled down the highest level of circ-Amotl1. Stat3 is a transcription factor-mediating signal transducer and activator of transcription 3. We confirmed this result by including antibody against AMOTL1, which was shown not to bind circ-Amotl1, and found that anti-Stat3 antibody bound only circ-Amotl1 (Figure 2B). We validated these results by preparing RNAs from the vector- and circ-Amotl1-transfected NIH 3T3 fibroblasts and performing pull-down assay. Anti-Stat3 antibody was found to pull down significantly higher levels of circ-Amotl1 from the circ-Amotl1-transfected cells than those from the vector-transfected cells (Figure 2C). To analyze the specificity of the interaction, we examined the levels of other circRNAs, including circ-DNSJA1, circ-MRPL47, circ-NDUF53, circ-RPS5, and circ-PRL5. We found that antibodies against Stat3 did not pull down these circRNAs (Figure 2D), suggesting specific interaction between circ-Amotl1 and Stat3.

We further tested the interaction between circ-Amotl1 and Stat3. Lysates from NIH 3T3 and HGF cells transfected with circ-Amotl1 or vector were mixed with a biotinylated probe specifically recognizing circ-Amotl1. The mixture was subject to real-time PCR, and the experiments showed that circ-Amotl1-transfected NIH 3T3 cells expressed high levels of circ-Amotl1 (Figure 2E, left). The mixture was subject to a pull-down assay by incubation with streptavidin beads, followed by real-time PCR, and we found that significantly higher levels of circ-Amotl1 were pulled down by the probe relative to the control (Figure 2E, right).

We tested whether the circ-Amotl1 probe was able to pull down Stat3. The probe was added to the lysates prepared from circ-Amotl1-transfected cells. Western blot analysis confirmed that transfection with circ-Amotl1 increased Stat3 levels (Figure 2F). The mixtures were incubated with streptavidin beads followed by western blotting, which showed that pulling down circ-Amotl1 precipitated Stat3 from cells transfected with circ-Amotl1 (Figure 2F).

To corroborate the interaction, we used a siRNA approach to knock down circ-Amotl1. Lysates prepared from HGFs transfected with circ-Amotl1 siRNA or a control oligo were mixed with the probes. Real-time PCR confirmed that transfection with circ-Amotl1 siRNA decreased circ-Amotl1 levels (Figure 2G, left). In the presence of the probe, significantly lower levels of circ-Amotl1 were pulled down (Figure 2G, right). In co-immunoprecipitation assay, pulling down circ-Amotl1 precipitated decreased levels of Stat3 from the circ-Amotl1 siRNA-transfected cells (Figure 2H).

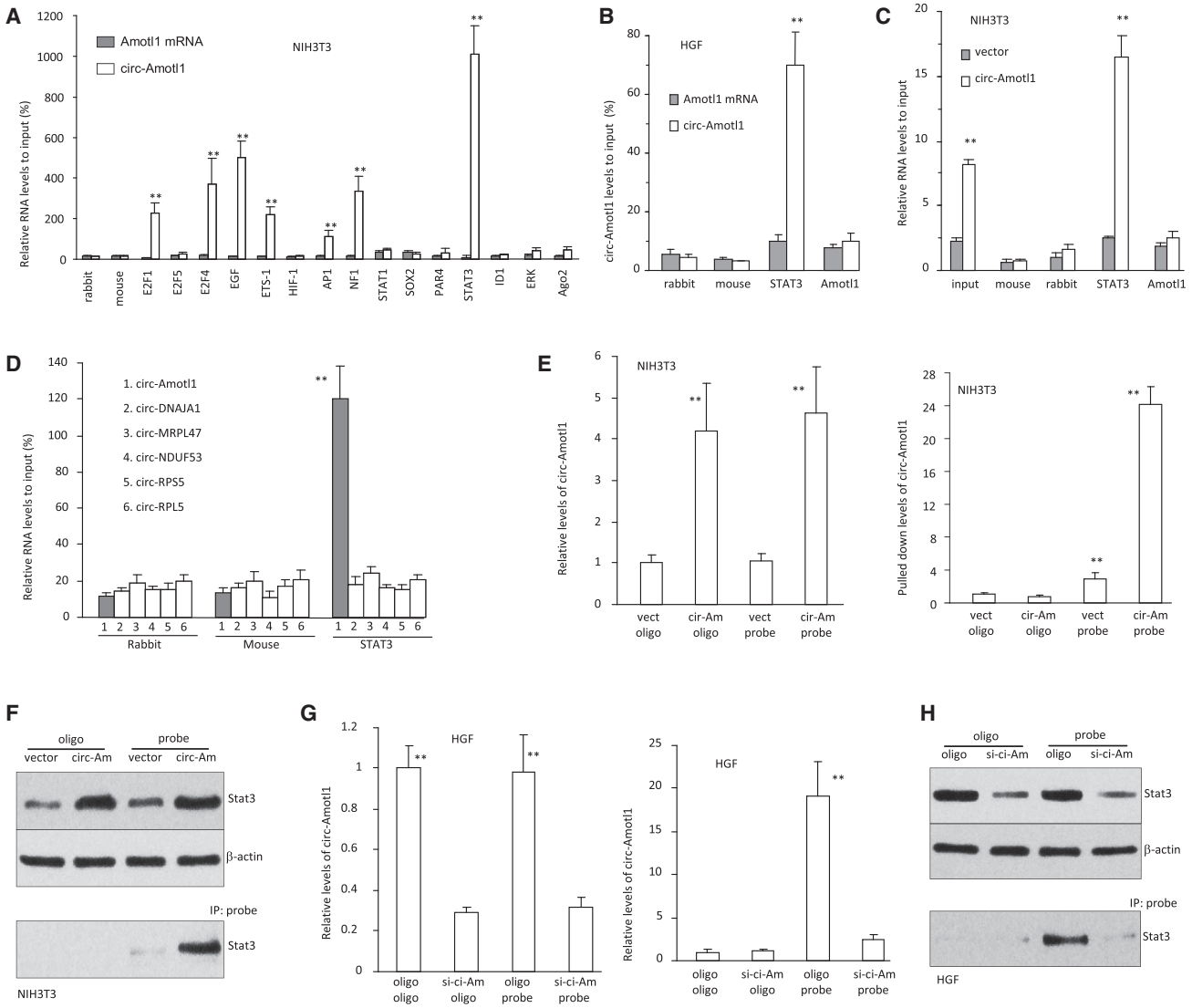

Figure 2. Interaction of circ-Amotl1 with Stat3

(A) Cell lysis prepared from NIH 3T3 cells was subjected to immunoprecipitation with rabbit IgG, mouse IgG, and antibodies as indicated, followed by real-time PCR with primers specific for linear Amotl1 mRNA or circ-Amotl1. Anti-Stat3 antibody pulled down the highest levels of circ-Amotl1 (n = 4). (B) RNAs isolated from HGF cells incubated with rabbit and mouse IgG, or antibody against STAT3 or AMOTL1, were subjected to real-time PCR. Anti-Stat3 antibody pulled down circ-Amotl1 but not Amotl1 mRNA (n = 4). (C) RNAs isolated from NIH 3T3 cells transfected with vector or circ-Amotl1 were subjected to real-time PCR. Anti-Stat3 antibody pulled down more circ-Amotl1 from the circ-Amotl1-transfected cells. (D) RNAs isolated from NIH 3T3 cells were subjected to real-time PCR with primers specific for circular RNAs as indicated. Antibodies against Stat3 pulled down circ-Amotl1 but not the other circular RNAs (n = 4). (E) Left: lysates prepared from NIH 3T3 transfected with circ-Amotl1 or mock control were mixed with biotinylated probes or a control oligo and then subjected to RNA pull-down assays. circ-Amotl1 transfection produced higher levels of circ-Amotl1 relative to control (n = 4). Right: the mixture was subjected to pull-down assays. circ-Amotl1 probe pulled down higher levels of circ-Amotl1 in the cells transfected with circ-Amotl1 (n = 4). (F) Protein lysates prepared from mock- and circ-Amotl1-transfected NIH 3T3 cells were subject to western blot probed with antibody against STAT3. Top: increased STAT3 levels in the circ-Amotl1-transfected cell lysate. Bottom: pull-down of Stat3 by the probe in lysates of the circ-Amotl1-tranbsfected cells. (G) Left: transfection with circ-Amotl1 siRNA silenced circ-Amotl1 expression. Right: real-time PCR showed that circ-Amotl1 probe pulled down less circ-Amotl1 in the cells transfected with circ-Amotl1 siRNA. **p < 0.01. Error bars denote SD (n = 4). (H) The probe pulled down less Stat3 in the siRNA-transfected cells compared with control.

Cross-Talk between circ-Amotl1 and Stat3

We explored how Stat3 might be mediating circ-Amotl1 function in cell migration and proliferation by screening potential targets of Stat3. Computational algorithm (http://bio.sz.tsinghua.edu.cn) prediction indicated that miR-17-5p was an excellent candidate in regulating Stat3 expression (Figure S2I). Our previous studies also showed that miR-17-5p could target fibronectin[18] and Dnmt3a.[19] We analyzed expression of miR-17-5p, Stat3, Dnmt3a, and fibronectin in the

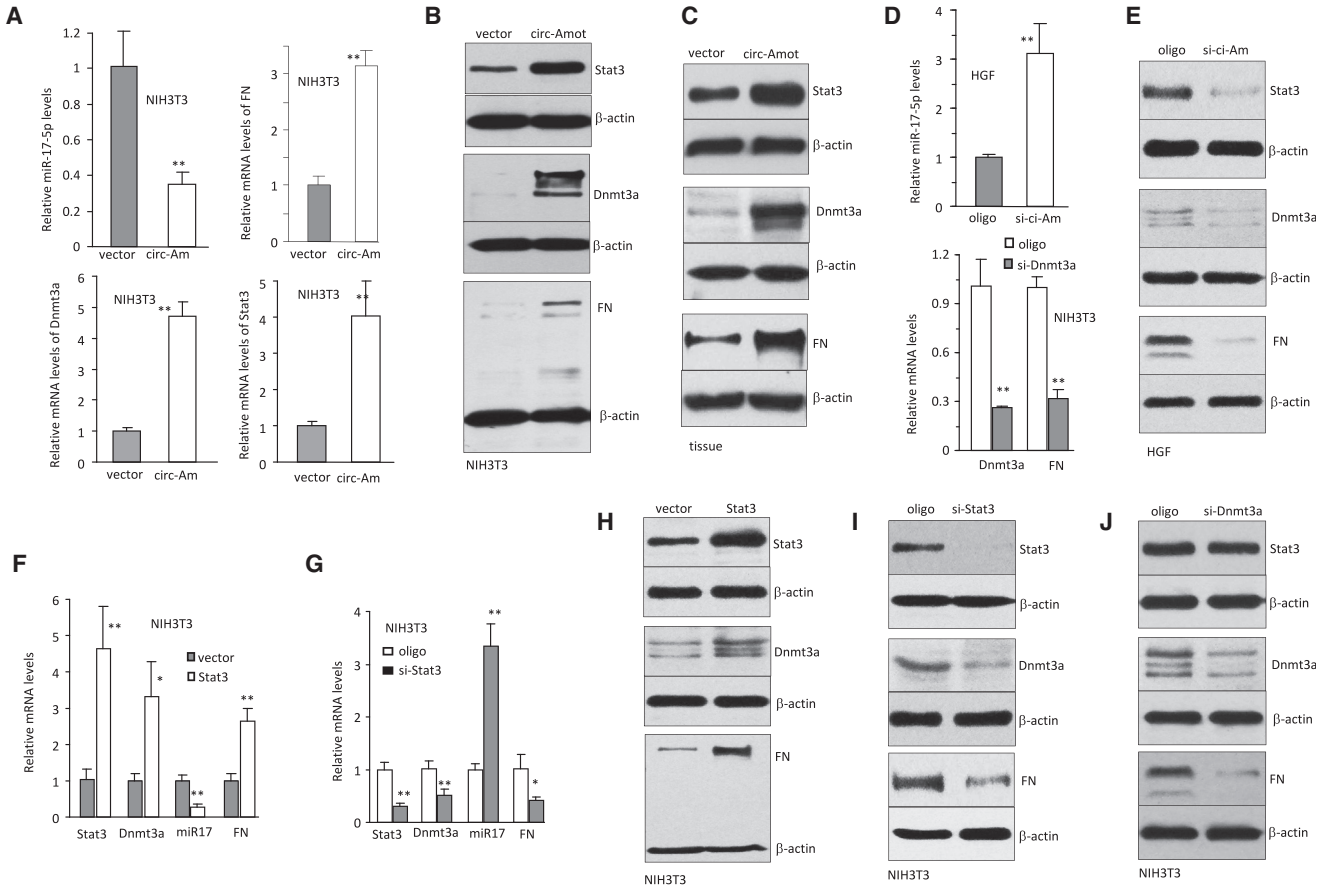

Figure 3. Crosstalk between circ-Amotl1 and Stat3

(A) In real-time PCR, downregulation of miR-17-5p and upregulation of fibronectin, Dnmt3a, and Stat3 levels were detected in the circ-Amotl1-transfected cells. **p < 0.01. Error bars denote SD (n = 4). (B) Transfected with circ-Amotl1 increased the expression of Stat3, Dnmt3a, and fibronectin (FN). (C) circ-Amotl1 injection increased the expression of Dnmt3a, fibronectin, and Stat3 in the wound tissues. (D) Top: real-time PCR showed that silencing circ-Amotl1 increased miR-17-5p expression. Bottom: silencing Dnmt3a decreased expression of Dnmt3a and fibronectin. (E) Western blotting confirmed that silencing circ-Amotl1 repressed expression of Stat3, Dnmt3a, and fibronectin. (F) Real-time PCR showed that ectopic expression of Stat3 increased the levels of Stat3, Dnmt3a, and fibronectin but decreased the levels of miR-17-5p. (G) Real-time PCR showed that silencing Stat3 decreased levels of Stat3, Dnmt3a, and fibronectin but increased levels of miR-17-5p. (H) Western blotting confirmed that ectopic expression of Stat3 increased expression of Dnmt3a and fibronectin. (I) Western blotting confirmed that silencing Stat3 decreased expression of Dnmt3a and fibronectin. (J) Western blotting confirmed that silencing Dnmt3a repressed expression of fibronectin but had no effect on Stat3 expression.

circ-Amotl1-transfected cells. We found that although miR-17-5p levels decreased, expression of Stat3, Dnmt3a, and fibronectin was upregulated in mRNA (Figure 3A) and protein levels (Figure 3B). In the wounds injected with circ-Amotl1, expression of Stat3, Dnmt3a, and fibronectin was also upregulated (Figures 3C and S2J). Consistently, silencing circ-Amotl1 increased miR-17-5p, and silencing Dnmt3a decreased fibronectin mRNA levels (Figure 3D). Silencing circ-Amotl1 decreased protein levels of Stat3, Dnmt3a, and fibronectin (Figure 3E).

We examined whether Dnmt3a and fibronectin were downstream molecules of Stat3. Real-time PCR analysis indicated that ectopic expression of Stat3 increased levels of Dnmt3a and fibronectin but decreased miR-17-5p expression (Figure 3F). Silencing endogenous Stat3 produced the opposite effect (Figure 3G). Western blot analysis confirmed that transfection with Stat3 increased Dnmt3a and fibronectin expression (Figure 3H), but silencing Stat3 decreased these protein levels (Figure 3I). Silencing Dnmt3a could clearly downregulated fibronectin expression (Figure 3J).

Effects of miR-17-5p on Wound Repair and Stat3 Expression

Because we have developed miR-17-transgenic mice in C57BL/6xCBA,[18,19] we used these mice, miR-17-transgenic and wild-type from the same litters, to explore the involvement of miR-17-5p in Stat3-mediated circ-Amotl1 function. Both male and female mice injected with circ-Amotl1 displayed accelerated wound healing. After confirmation of miR-17-5p upregulation (Figure S3A), the mice were subjected to a cervical dermal punch wounds of about 5 mm on both sides of the back. The sizes of the wound areas were measured as above. It appeared that the miR-17-transgenic mice showed delay in wound healing (Figure S3B). The difference in wound area between

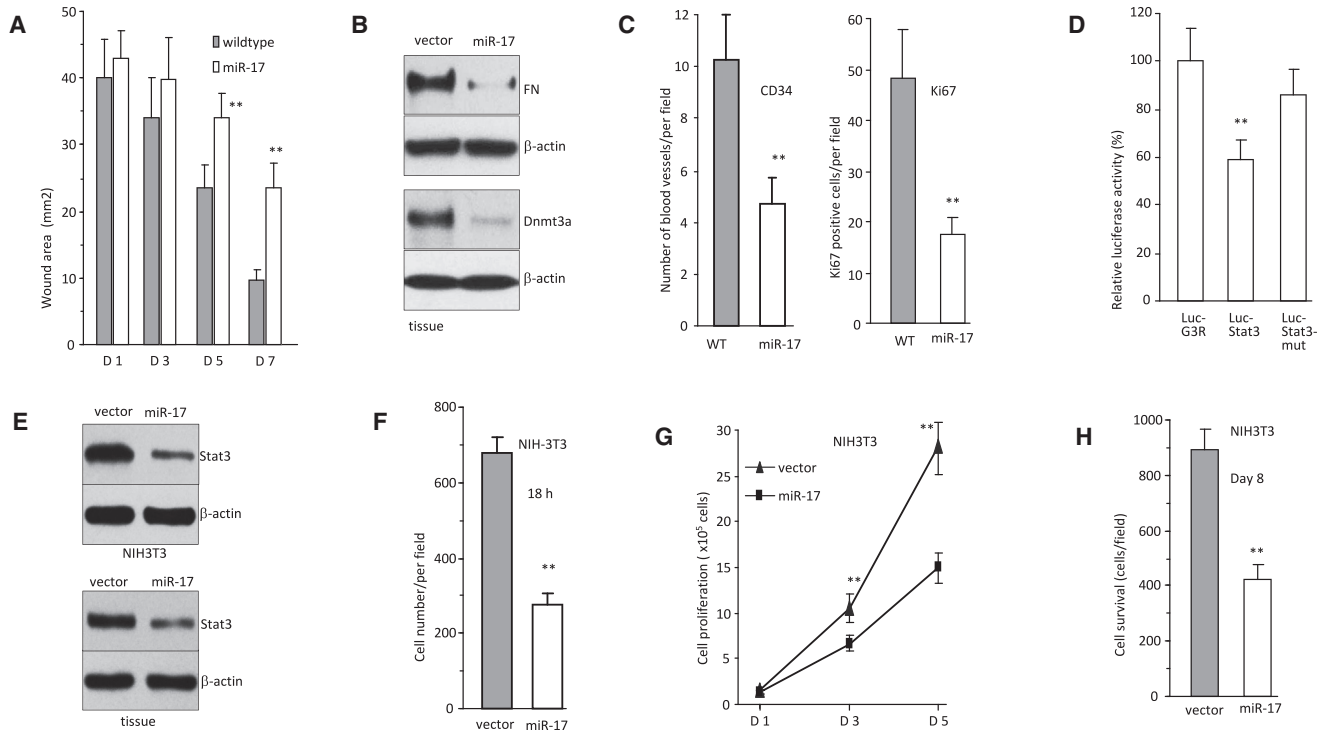

Figure 4. Effects of miR-17-5p on Wound Healing and Stat3 Expression

(A) The miR-17-transgenic and wild-type (from the same letters) mice were subject to wound healing assay (n = 10). Graphical representation of wound sizes showing that miR-17 transgenic mice had larger wounds than wild-type mice after 5 and 7 days. (B) The wound tissues were subject to western blotting to confirm repression of fibronectin and Dnmt3a in the miR-17 transgenic mice. (C) Quantitation analysis showed decreased levels of CD34 and Ki67 in the miR-17 transgenic mice. **p < 0.01. Error bars denote SD (n = 5). (D) Decreased luciferase activities were observed in cells co-transfected with miR-17-5p and Luc-stat3, which was reversed when the miR-17-5p binding site was mutated (Luc-stat3-mut) (n = 4). (E) Protein lysates from NIH 3T3 cells transfected with miR-17-5p and control oligo (top) or the wound tissues of miR-17 transgenic mice and wild-type mice (bottom) were subjected to immunoblotting. MiR-17 expression decreased Stat3 levels. (F) MiR-17 expression decreased cell migration in the trans-well assay compared with control (n = 5). (G) Ectopic expression of miR-17-5p repressed cell proliferation (n = 5). (H) In serum-free medium, miR-17 expression decreased cell survival (n = 5).

two groups was statistically significant (Figure 4A). The ratios of unhealed space (day 5/day 1 and day 7/day 1) were significantly greater in the miR-17-transgenic mice than that in the wild-type mice 5 days after wounding (Figure S3C).

On the seventh day, the wounded tissues were biopsied for western blotting, histological examination, and immunohistochemistry staining. H&E staining showed that there was decreased cell density in the wounds of miR-17-transgenic mice, compared with the wild-type (Figure S3D). Western blot analysis confirmed repression of fibronectin and Dnmt3a (Figure 4B). We also found that there were fewer CD34- and Ki67-positive cells in the miR-17 transgenic mice (Figure S3E). Quantitation of the numbers of stained blood vessels and Ki67-positive cells showed significant decrease in the miR-17-transgenic mice (Figure 4C).

In our previous studies, we showed that expression of miR-17-5p repressed expression of Dnmt3a and fibronectin.[18,19] Our results reported here suggested that Stat3 was a target of miR-17-5p. We tested this by generating luciferase constructs harboring the 3′UTR of Stat3. Site-directed mutagenesis was also performed in the miR-17-5p binding site. Luciferase assay indicated that luciferase activity was repressed when the cells were co-transfected with the luciferase construct and miR-17-5p (Figure 4D). The inhibitory effect was abolished when the miR-17-5p binding site was mutated. Western blotting showed that in the cells stably transfected with miR-17 (Figure S3F, confirming upregulation of miR-17-5p), levels of Stat3 were repressed (Figure 4E). The effects of miR-17 transfection were found to decrease 2D (Figure S3G) and 3D (Figures 4F and S3H) cell migration, cell proliferation (Figure 4G), and survival (Figure 4H). We confirmed that expression of Stat3, Dnmt3a, and fibronectin was downregulated in the miR-17-transgenic mice (Figure S3I).

Mutual Regulation of circ-Amotl1, Stat3, Dnmt3a, Fibronectin, and miR-17-5p

We then designed experiments to address how circ-Amotl1 increased Dnmt3a expression. Because Stat3 is a transcription factor, we proposed that circ-Amotl1 bound to Stat3 and Dnmt3a promoter, facilitating Dnmt3a transcription (Figure 5A). Experiments were conducted to validate this proposal. We found that the expressed

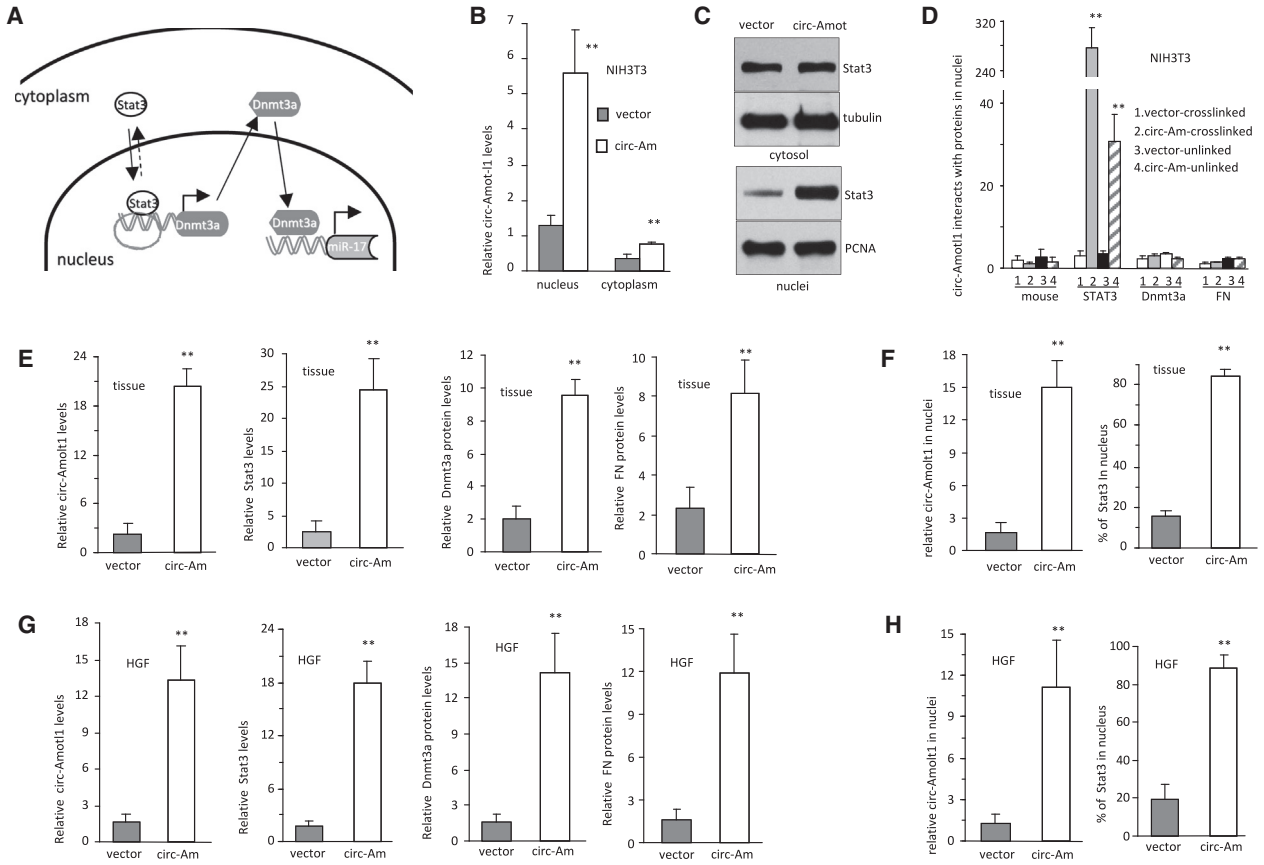

Figure 5. Effects of circ-Amotl1 on Stat3 Nuclear Translocation

(A) A diagram showing that expression of circ-Amotl1 enhanced Stat3 nuclear translocation, which promoted Dnmt3a transcription. Increased Dnmt3a expression repressed miR-17 transcription. (B) Real-time PCR showed that significantly higher levels of circ-Amotl1 were detected in the nuclei compared with the cytoplasm (n = 4). (C) Western blotting showed that ectopic expression of circ-Amotl1 increased Stat3 levels in the nucleus but not in the cytoplasm. (D) Cell nuclear lysis prepared from NIH 3T3 cells was subjected to immunoprecipitation, followed by real-time PCR. Anti-Stat3 antibody pulled down significantly higher levels of circ-Amotl1 when the samples were pre-treated with crosslinking (n = 6). (E) Quantitation of circ-Amotl1, Stat3, Dnmt3a, and fibronectin in wound tissues injected with circ-Amotl1 or the control plasmid. (F) Quantitation of nuclear translocation of circ-Amotl1 and Stat3 in the wound tissues. (G) Quantitation of circ-Amotl1, Stat3, Dnmt3a, and fibronectin in HGF cells transfected with circ-Amotl1 or the vector. (H) Quantitation of nuclear translocation of circ-Amotl1 and Stat3 in HGF cells.

circ-Amotl1 was translocated mainly to the nucleus (Figure 5B), and the upregulated Stat3 was seen mainly in the nucleus (Figure 5C). In the crosslinking assays, we found that circ-Amotl1 was precipitated by anti-Stat3 antibody but not the other antibodies (Figure 5D).

Confocal microscopic analysis detected mainly nuclear distribution of Stat3 in the circ-Amotl1-injected wound tissues (Figure S4A). Using a probe specifically recognizing circ-Amotl1, we detected co-localization of circ-Amotl1 and Stat3 in the nuclei of the circ-Amotl1-injected tissues. Expression of Dnmt3a and fibronectin increased in the wound tissues delivered with circ-Amotl1 (Figure S4B). Quantification analysis showed that expression of circ-Amotl1, Stat3, Dnmt3a, and fibronectin increased in the wound tissues delivered with circ-Amotl1 (Figure 5E). The levels of circ-Amotl1 and Stat3 were significantly higher in the nuclei of the circ-Amotl1-treated tissues relative to the vector-treated tissues (Figure 5F). In the circ-Amotl1-transfected cells, we detected increased expression of circ-Amotl1, Stat3, Dnmt3a, and fibronectin (Figures 5G and S5A), and nuclear translocation of circ-Amotl1 and Stat3 (Figures 5H and S5B).

We tested the interaction between Stat3 and Dnmt3a promoter in the cells transfected with circ-Amotl1 or the vector. Chromatin was isolated, digested, and immunoprecipitated with antibodies against Stat3, Histone H3 (serving as a positive control), and rabbit IgG (serving as a negative control), followed by PCR with primers flanking a fragment of DNA in the Dnmt3a promoter. It showed that antibody against Stat3 pulled down significantly higher levels of Dnmt3a promoter in the presence of circ-Amotl1 than in the control (Figure 6A). We further examined the effect of Stat3 on the interaction with Dnmt3a promoter by ectopic expression of Stat3 expression construct. Ectopic expressed Stat3 increased pulling down the DNA

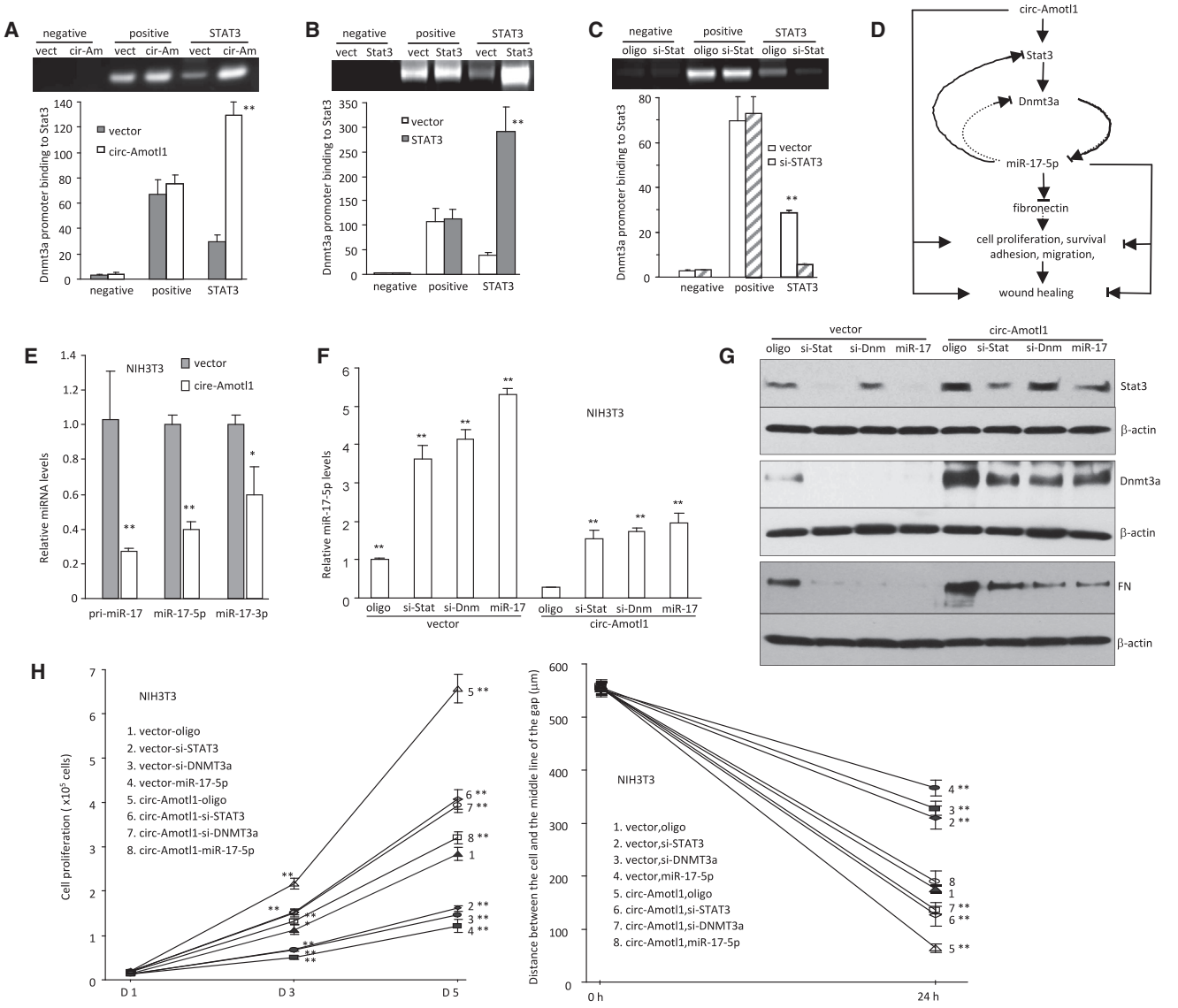

Figure 6. Effect of circ-Amotl1 on Wound Healing

(A) Top: increased interaction of Stat3 with Dnmt3a promoter in the circ-Amotl1-transfected cells. Bottom: quantitation analysis (n = 4). (B) Increased interaction of Stat3 with Dnmt3a promoter in the Stat3-transfected cells. (C) Decreased interaction of Stat3 with Dnmt3a promoter in the cells transfected with Stat3 siRNA (n = 4). (D) The pathway by which circ-Amotl1 affected wound healing. (E) Real-time PCR showed that expression of circ-Amotl1 decreased levels of pri-miR-17, miR-17-5p, and miR-17-3p compared with the vector. *$p < 0.05$, **$p < 0.01$. Error bars denote SD (n = 5). (F) circ-Amotl1- and vector-transfected NIH 3T3 cells were transfected with control oligo, miR-17-5p, Stat3 siRNA, and Dnmt3a siRNA. Transfection with miR-17-5p or silencing Stat3 and Dnmt3a repressed expression of miR-17-5p in the circ-Amotl1-transfected cells. (G) Western blot showed that transfection with miR-17-5p or silencing Stat3 and Dnmt3a increased expression of Stat3, Dnmt3a, and fibronectin in the circ-Amotl1-transfected cells relative to the vector-transfected cells. (H) Upregulation of Stat3, Dnmt3a, and fibronectin in the cells transfected with circ-Amotl1 displayed higher rates of proliferation (left) and migration (right).

promoter (Figure 6B). Silencing endogenous Stat3 decreased pulling down the promoter (Figure 6C).

On the basis of the above results, we proposed that ectopic expression of circ-Amotl1 increased Stat3 expression. Increased Stat3 levels enhanced Dnmt3a expression. Dnmt3a could then methylate miR-17 gene promoter. Because Stat3, Dnmt3a, and fibronectin are the targets of miR-17-5p, decreased miR-17-5p levels would increase expression of fibronectin, Dnmt3a, and Stat3. All of these activities led to increased cell proliferation, survival, migration, and wound repair (Figure 6D). A few key experiments were performed to further validate this proposed mode of action. We examined whether ectopic

expression of circ-Amotl1 would decrease primary miR-17, miR-17-5p, and miR-17-3p, and our experiment confirmed this (Figure 6E). We transfected the circ-Amotl1- and vector-stable cell lines with Dnmt3a siRNA, Stat3 siRNA, miR-17-5p, or a control oligo. Real-time PCR analysis indicated that the miR-17-5p levels were upregulated in the cells transfected with siRNAs targeting Stat3 or Dnmt3a (Figure 6F). We also found upregulation of Stat3, Dnmt3a, and fibronectin in the cells transfected with circ-Amotl1 (Figure 6G). These cells also displayed higher rates of proliferation and migration relative to the controls (Figure 6H).

Computational Analysis of circ-Amotl1 Interacting with Stat3

In silico, we found that Stat3 shared consensus sequences with other RNA-binding proteins (Figure 7A). The predicted secondary structure of circ-Amotl1 was obtained by analyzing its thermodynamic properties using the formula $\Delta G = \Delta H - T\Delta S$, where $\Delta G = -14.70$ kcal/mol at 37°C, $\Delta H = -380.00$ kcal/mol, and $\Delta S = -1{,}177.8$ cal/(K·mol), T (K) is the absolute temperature, and ΔG, ΔH, and ΔS denote the changes in free energy, enthalpy, and entropy, respectively. The secondary structure delineated in dot bracket notation was then analyzed using the software RNAComposer for tertiary structure prediction. Finally, NPDock was used to carry out the in silico molecular docking of circ-Amotl1 with Stat3 (Figures 7B and S6A). The Stat3 used in the docking procedure was derived from Protein Data Bank (PDB) entry 1BG1. The molecular simulation result supports that circ-Amotl1 could perfectly dock Stat3 and predicts a minimal binding region of circ-Amotl1 for Stat3: 'AACCTTCAC"AAC"AGGAAGAA'. The contact map (Figure S6B), the residue-level resolution contact maps (Figure S6C), the MC score (Figure S6D), the contact distance (Table S1), the accessible surface area (Table S2), and the interaction overview (Table S3) all supported the conclusion that circ-Amotl1 sufficiently docked Stat3.

To evaluate the effects of the binding sites on mediating circ-Amotl1 functions, we designed blocking oligo complementary to the binding sites (Figure 7C). NIH 3T3 cells expressing circ-Amotl1 were transfected with blocking oligo inhibiting circ-Amotl1-Stat3 interaction, followed by western blotting. We detected decreased levels and nuclear translocation of Stat3 (Figure 7D). As well, expression of Dnmt3a and fibronectin decreased. The cells transfected with the blocking oligo also displayed decreased proliferation, survival, and migration (Figure 7E) but increased levels of miR-17-5p (Figure 7F) relative to circ-Amotl1-transfected cells. We confirmed that the probe pulled down equal amounts of circ-Amotl1 (Figure 7G), but it pulled down a decreased amount of Stat3 (Figure 7H) in the presence of the blocking oligo.

To corroborate these results, we delivered the blocking oligo or the control oligo into HGF cells to test the effect of endogenous circ-Amotl1. We found that transfection with the blocking oligo decreased levels and nuclear translocation of Stat3 and decreased expression of Dnmt3a and fibronectin (Figure 7I) but increased miR-17-5p expression (Figure 7J). Delivery of the blocking oligo decreased proliferation, survival, and migration (Figure 7K).

DISCUSSION

In this study, we demonstrated that delivery of a circRNA circ-Amotl1 enhanced wound repair by promoting cell proliferation, survival, adhesion, and migration. The increased cell activities occurred through circ-Amotl1 enhancing nuclear translocation of Stat3. Nuclear Stat3 could then bind to Dnmt3a promoter, facilitating transcription and translation of Dnmt3a. Dnmt3a induced methylation of miR-17 promoter, decreasing miR-17-5p expression. We have previously identified Dnmt3a and fibronectin as the targets of miR-17-5p.[1,18] In the present study, we identified Stat3 as the miR-17-5p target. Thus, decreased expression of miR-17-5p promoted protein expression of these targets, which was validated by a number of experiments including western blotting, luciferase assay, and immunostaining. Increased expression of these proteins led to promotion of cell proliferation, survival, adhesion, and migration, which led to acceleration of wound repair.

circRNAs have recently emerged as a novel class of non-coding RNAs. Their biological functions are largely unknown. Several studies have shown that circRNAs can function as sponges to regulate miRNA activities.[1,7,13,15] We have also found that circRNA circ-Foxo3 repressed cell cycle progression by binding to p21 and CDK2[4] and enhanced cell senescence by binding to a number of proteins associated with stress and senescent responding factors.[2] Although circRNAs have been detected in mammalian cells for a few years, the number of circRNAs has been found to be more than that of mRNAs. It is conceivable that circRNAs may play roles in regulating a variety of physiological activities. Our study reported here shows that delivery of circ-Amotl1 to wound tissues accelerated wound repair. Our mouse wound healing model did not contain the splinting step, compared with the mouse excisional wound splinting model. This would facilitate wound healing faster, allowing us to measure the effect of circ-Amotl1 more effectively. In the mouse excisional wound splinting model, much more time is needed to heal the wound, which would require many more injections of the plasmids and could generate greater deviation technically. In future studies using transgenic mice overexpressing circRNAs, the mouse excisional wound splinting model would better mimic human skin wound healing.

Wound repair is achieved by complex and active physiological processes.[20–22] In the wound, leukocytes are responsible for immune response, while keratinocytes generate epithelial cover, and fibroblasts produce contractile forces between cell-cell and cell-ECM conjunctions.[23,24] These cells are actively taking up nutrition from the environment and producing building blocks for the healing process.[25] This allows effective uptake of the delivered circRNA-expressing plasmids, and we did detect extensive expression of circ-Amotl1 in the wound tissues. Our model appears to be an ideal one for tissue regeneration, especially for topical application to the wound. Because the expressed product is a natural component of the cell, this approach may have few side effects on the body.

One important aspect of our study is that each circ-Amotl1-transfected NIH 3T3 fibroblast could grow well in single-cell culture

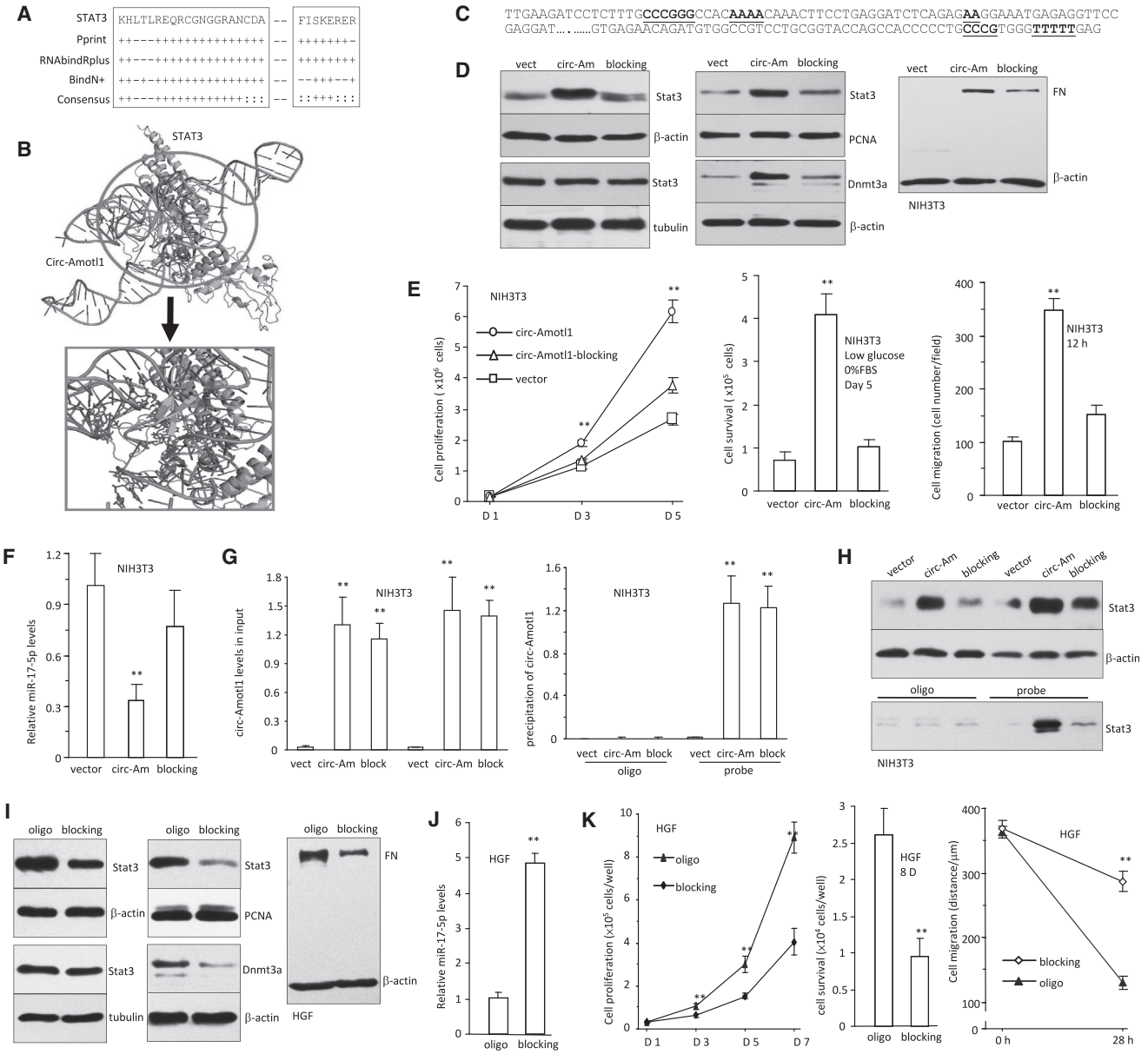

Figure 7. circ-Amotl1 Interacting with Stat3

(A) Prediction of probable RNA-binding residues of Stat3 was carried out by submitting the Stat3 sequence to Pprint, RNABindRPlus, and BindN+ servers. Plus signs indicate the predicted RNA-binding residues. (B) Graphical representation of 3D structures of the docking models of circ-Amotl1 with Stat3 and zoomed-in images of the binding interface done by NPDcok (color graphic provided in Figure S6A). (C) circ-Amotl1 sequence labeling Stat3 binding site (red). (D) Delivery of the blocking oligo repressed expression of Stat3, Dnmt3a, and fibronectin and nuclear translocation of Stat3. (E) Delivery of the blocking oligo decreased cell proliferation (left), survival (middle), and migration (right). (F) Expression of miR-17-5p was enhanced by the blocking oligo. (G) In the presence of the blocking oligo, expression of circ-Amotl1 was not affected (left), and the probe could still precipitate equal amounts of circ-Amotl1 (right). (H) In the presence of the blocking oligo, the probe pulled down decreased levels of Stat3. (I) The blocking oligo inhibited expression of Stat3, Dnmt3a, and fibronectin and nuclear translocation of Stat3. (J) The blocking oligo increased miR-17-5p expression. (K) Delivery of the blocking oligo decreased cell proliferation (left), survival (middle), and migration (right).

relative to the vector control. We developed a single-cell culture experiment to mimic the early stage of wound repair, when the cells are sparse and most of the cells are far away from one another. We found that the vector-transfected fibroblasts either died or grew slowly when they were maintained individually one cell per well. However, most of the circ-Amotl1-transfected cells could survive and grew fast. This acquired property allowed the wound to heal effectively.

In looking for protein that might be mediating circ-Amotl1 effects, we performed a binding assay with antibodies against a number proteins involved in the pathways of cell proliferation, survival, adhesion, and migration. It was found that Stat3 appeared to bind circ-Amotl1 with highest activity, as Stat3 plays important role in regulating cell activity.[26–28] Because several other proteins, including E2F1, E2F4, FGF, ETS-1, and NF1, could also bind to circ-Amotl1 significantly, we cannot exclude the possibility that some of these proteins may also play roles in mediating the role of circ-Amotl1 in wound healing. This awaits future investigation. Nevertheless, the interaction of circ-Amotl1 with Stat3 appeared to be specific, as other circRNAs tested could not bind to Stat3.

Our results that circ-Amotl1 could regulate miR-17-5p expression and that miR-17-5p could repress Stat3 levels, resulting in downregulation of circ-Amotl1 function, have added an additional layer to understanding of the mutual regulation of these two classes of non-coding RNAs. Previous studies have shown that circRNAs can sponge miRNAs and decrease their activities, but it is not known whether miRNAs can regulate circRNA activities. Our results show a feedback loop in the mutual regulation of Stat3 and miR-17-5p expression, suggesting a mutual regulation of circ-Amotl1 and miR-17-5p functions.

MATERIALS AND METHODS

Materials

The monoclonal or polyclonal antibodies against Ki67 (550609; BD Pharmingen), CD34 (ab81289; Abcam), Dnmt3a (ab23565; Abcam), fibronectin (ab2413; Abcam) were obtained from different sources as indicated. Horseradish peroxidase-conjugated goat anti-mouse IgG and horseradish peroxidase-conjugated goat anti-rabbit IgG were obtained from Bio-Rad. RNA and DNA extraction kits and RNA RT and PCR kits were obtained from QIAGEN. Immunoblotting was performed using the ECL western blot detection kit (Amersham Biosciences). Protein A-Sepharose 4B Conjugate and Dynabeads MyOne Streptavidin C1 magnetic beads were obtained from Invitrogen.

In Vivo Wound Healing Experiment with circ-Amotl1

A circ-Amotl1 expression construct was generated by our lab. The plasmids contained a Bluescript backbone, a CMV promoter driving circ-Amotl1 or a non-related sequence serving as a control, and the GFP expression unit. All primer sequences used are listed in Figure S6E.

At 4 weeks of age, 10 miR-17 transgenic and 10 wild-type mice of both genders were subject to skin biopsy using a punch (Miltex) of 5 mm in diameter. The transgenic mice were generated by our lab as previously described.[18] A pair of full-thickness, excisional wounds were created on the dorsal region of each mouse. Wound size was measured by multiplying longest length by greatest width, and all mice were sacrificed 1 week afterward. Tissue samples were collected for further study. Using similar procedure, we also created wounds followed by injection of circ-Amotl1 plasmids or a control vector at a volume of 100 μL containing 50 μg plasmids per site. All experimental procedures were approved by the Animal Care Committee of Sunnybrook Research Institute and followed current law regarding animal protection.

Synthesis of the deliver complexes (plasmid-PEG-Au NP) was performed as previously described.[29–32] Briefly, 500 μg circ-Amotl1 plasmid was dissolved in 800 μL of RNase-free water. mPEGSH (PG1-TH-2k; Nanocs) was mixed with plasmids (1:20 molar ratio). Then, 10 nm gold nanoparticles (AuNP; Cytodiagnostics) were mixed with plasmid-PEG at a weight ratio of 1:1 for conjugation. The mixture was gently shaken at 60°C for 30 min and then transferred into a syringe for local injection into the wound tissues.

Cell Adhesion and Migration Assays

In adhesion assays, 1×10^6 cells were seeded in Petri dishes with 10% or 25% FBS/DMEM and maintained at 37°C. Pictures were taken in randomly selected high-power fields under an inverted light microscope (Carl Zeiss Microscopy), and cell numbers were counted at 4 or 6 hr. Cell migration was performed by wound healing and transwell assays. In wound healing assays, NIH 3T3 fibroblasts were seeded in 6-well plates at a density of 1×10^6 cells/well for 12 hr. To diminish the influence of proliferation, the cells were treated with Mitomycin C (Sigma-Aldrich) at 10 μg/mL for 2 hr before being changed to serum-free media. The cultures were then scraped linearly with 200 μL micropipette tips (BioMart). At 0, 18, and 24 or 30 hr, cell migration patterns were recorded by inverted light microscopy, and the migration distance was measured and quantified. In order to test cell motility in a 3D way, PET track-membrane (Coster; Sigma-Aldrich) was placed in 24-well tissue culture dishes, and 1×10^5 cells in 100 μL media without FBS were loaded into the upper part of the membrane. The lower portions of the wells were filled with 800 μl DMEM containing 10% FBS. After incubation at 37°C for 4, 10, 12, or 18 hr, nonmigrated cells were removed with a cotton swab, and invaded cells were fixed by 100% methanol for 30 min, followed by staining with Coomassie Brilliant Blue (Bio-Rad) for 10 min. Photographs were taken under an inverted light microscope.

Cell Proliferation and Survival Assays

Cells (NIH 3T3, 1×10^5 cells; HGF, 2×10^4 cells) were seeded in 6-well or 12-well cell culture plates with 10% or 25% FBS/DMEM and maintained at 37°C for 5 or 7 days. Cell number was counted every other day.[33] Single-cell proliferation was performed as previously described.[34] To test cell survival, 1×10^5 cells were seeded in 6-well dishes, cultured in 10% (NIH 3T3 cells) or 25% (HGF cells) FBS/DMEM, and maintained at 37°C. After 12 hr of culture, the medium was removed, and the cultures were washed with PBS two times, followed by addition of serum-free DMEM. Pictures were taken in randomly selected high-power fields under an inverted light microscope, and cell number was counted on day 5, 8, or 18.

Chromatin Immunoprecipitation Assay

Chromatin immunoprecipitation (ChIP) was performed using the SimpleChIP chromatin IP kit (Cell Signaling Technology) according to the manufacturer's instructions. Briefly, cells were treated with

formaldehyde solution, and the chromatin was isolated, digested, and immunoprecipitated with antibody against Stat3. A total of 10% of the inputs were used for immunoblotting. The captured chromatin was eluted, crosslinking was reversed, and the DNA was recovered. ChIP DNA was subject to PCR using specific primers flanking a DNA sequence in the promoter region of Dnmt3a.

Protein and RNA Analyses

For preparation of nuclei, cells were lysed in 1 mL nuclear extraction buffer (20 mM HEPES, pH 7.2, 10 mM KCl, 2 mM $MgCl_2$, and 10 μL PI) and homogenized with a prechilled Dounce homogenizer with 20 strokes. The lysis was centrifuged at 4,200 rpm for 5 min. The pellet was washed with PBS five times and resuspended in 100 μL lysis buffer containing 0.5 M NaCl. After centrifugation at 13,000 rpm for 10 min, the supernatants containing nuclear extract were collected for analysis.

Protein analysis on western blotting was performed as previously described.[35] Immunohistochemistry was performed in tissue sections as previously described.[30,36] Real-time PCR analysis of RNAs was performed as previously described.[1,37] The procedures for protein precipitating RNA and RNA pull-down proteins were performed as previously described.[19] Fluorescence in situ hybridization (FISH) was performed as previously described.[38] NIH 3T3 cells were seeded in 12-well tissue culture dishes at a density of 1×10^5 cells/well. The cells were co-transfected with the luciferase reporter constructs and miR-17-5p duplex, using Lipofectamine 2000. Luciferase activity was performed as previously described.[35]

Statistical Analysis

All experiments were performed in triplicate, and numerical data were subject to independent-samples t tests. Levels of significance were set at $^*p < 0.05$ and $^{**}p < 0.01$.

SUPPLEMENTAL INFORMATION

Supplemental Information includes six figures and three tables and can be found with this article online at http://dx.doi.org/10.1016/j.ymthe.2017.05.022.

AUTHOR CONTRIBUTIONS

Z.-G.Y., W.W.D., Y.Z., J.L., and S.G. performed the experiments. F.M.A. performed computational analysis. Z.-G.Y., W.W.D., W.Y., and B.B.Y. designed the project and experiments. Z.-G.Y., W.Y., and B.B.Y. wrote the paper.

CONFLICTS OF INTEREST

The authors declare no conflict of interest.

ACKNOWLEDGMENTS

This work was supported by the Canadian Institutes of Health Research (grant PJT-149083) to B.B.Y., who is the recipient of a Career Investigator Award (CI7418) from the Heart and Stroke Foundation of Ontario. Z.-G.Y. is supported by a scholarship from the China Scholarship Council. W.W.D. is supported by a postdoctoral fellowship from the Breast Cancer Foundation of Ontario. F.M.A. is supported by the Higher Education Commission of Pakistan.

REFERENCES

1. Yang, W., Du, W.W., Li, X., Yee, A.J., and Yang, B.B. (2016). Foxo3 activity promoted by non-coding effects of circular RNA and Foxo3 pseudogene in the inhibition of tumor growth and angiogenesis. Oncogene *35*, 3919–3931.
2. Du, W.W., Yang, W., Chen, Y., Wu, Z.K., Foster, F.S., Yang, Z., Li, X., and Yang, B.B. (2017). Foxo3 circular RNA promotes cardiac senescence by modulating multiple factors associated with stress and senescence responses. Eur. Heart J. *38*, 1402–1412.
3. Xie, Y.Z., Yang, F., Tan, W., Li, X., Jiao, C., Huang, R., and Yang, B.B. (2016). The anti-cancer components of Ganoderma lucidum possesses cardiovascular protective effect by regulating circular RNA expression. Oncoscience *3*, 203–207.
4. Du, W.W., Yang, W., Liu, E., Yang, Z., Dhaliwal, P., and Yang, B.B. (2016). Foxo3 circular RNA retards cell cycle progression via forming ternary complexes with p21 and CDK2. Nucleic Acids Res. *44*, 2846–2858.
5. Zhang, Y., Zhang, X.O., Chen, T., Xiang, J.F., Yin, Q.F., Xing, Y.H., Zhu, S., Yang, L., and Chen, L.L. (2013). Circular intronic long noncoding RNAs. Mol. Cell *51*, 792–806.
6. Wang, P.L., Bao, Y., Yee, M.C., Barrett, S.P., Hogan, G.J., Olsen, M.N., Dinneny, J.R., Brown, P.O., and Salzman, J. (2014). Circular RNA is expressed across the eukaryotic tree of life. PLoS ONE *9*, e90859.
7. Hansen, T.B., Jensen, T.I., Clausen, B.H., Bramsen, J.B., Finsen, B., Damgaard, C.K., and Kjems, J. (2013). Natural RNA circles function as efficient microRNA sponges. Nature *495*, 384–388.
8. Li, Z., Huang, C., Bao, C., Chen, L., Lin, M., Wang, X., Zhong, G., Yu, B., Hu, W., Dai, L., et al. (2015). Exon-intron circular RNAs regulate transcription in the nucleus. Nat. Struct. Mol. Biol. *22*, 256–264.
9. Jeck, W.R., Sorrentino, J.A., Wang, K., Slevin, M.K., Burd, C.E., Liu, J., Marzluff, W.F., and Sharpless, N.E. (2013). Circular RNAs are abundant, conserved, and associated with ALU repeats. RNA *19*, 141–157.
10. Jakobi, T., Czaja-Hasse, L.F., Reinhardt, R., and Dieterich, C. (2016). Profiling and validation of the Circular RNA repertoire in adult murine hearts. Genomics Proteomics Bioinformatics *14*, 216–223.
11. Salzman, J., Chen, R.E., Olsen, M.N., Wang, P.L., and Brown, P.O. (2013). Cell-type specific features of circular RNA expression. PLoS Genet. *9*, e1003777.
12. Burd, C.E., Jeck, W.R., Liu, Y., Sanoff, H.K., Wang, Z., and Sharpless, N.E. (2010). Expression of linear and novel circular forms of an INK4/ARF-associated non-coding RNA correlates with atherosclerosis risk. PLoS Genet. *6*, e1001233.
13. Zheng, Q., Bao, C., Guo, W., Li, S., Chen, J., Chen, B., Luo, Y., Lyu, D., Li, Y., Shi, G., et al. (2016). Circular RNA profiling reveals an abundant circHIPK3 that regulates cell growth by sponging multiple miRNAs. Nat. Commun. *7*, 11215.
14. Liu, Q., Zhang, X., Hu, X., Dai, L., Fu, X., Zhang, J., and Ao, Y. (2016). Circular RNA related to the chondrocyte ECM regulates MMP13 expression by functioning as a MiR-136 'sponge' in human cartilage degradation. Sci. Rep. *6*, 22572.
15. Li, F., Zhang, L., Li, W., Deng, J., Zheng, J., An, M., Lu, J., and Zhou, Y. (2015). Circular RNA ITCH has inhibitory effect on ESCC by suppressing the Wnt/β-catenin pathway. Oncotarget *6*, 6001–6013.
16. Capel, B., Swain, A., Nicolis, S., Hacker, A., Walter, M., Koopman, P., Goodfellow, P., and Lovell-Badge, R. (1993). Circular transcripts of the testis-determining gene Sry in adult mouse testis. Cell *73*, 1019–1030.
17. Shu, Y.Y., and Maibach, H.I. (2011). Estrogen and skin: therapeutic options. Am. J. Clin. Dermatol. *12*, 297–311.
18. Shan, S.W., Lee, D.Y., Deng, Z., Shatseva, T., Jeyapalan, Z., Du, W.W., Zhang, Y., Xuan, J.W., Yee, S.P., Siragam, V., and Yang, B.B. (2009). MicroRNA miR-17 retards tissue growth and represses fibronectin expression. Nat. Cell Biol. *11*, 1031–1038.
19. Du, W.W., Yang, W., Xuan, J., Gupta, S., Krylov, S.N., Ma, X., Yang, Q., and Yang, B.B. (2016). Reciprocal regulation of miRNAs and piRNAs in embryonic development. Cell Death Differ. *23*, 1458–1470.

20. Al Haj Zen, A., Nawrot, D.A., Howarth, A., Caporali, A., Ebner, D., Vernet, A., Schneider, J.E., and Bhattacharya, S. (2016). The retinoid agonist tazarotene promotes angiogenesis and wound healing. Mol. Ther. *24*, 1745–1759.

21. Kühl, T., Mezger, M., Hausser, I., Handgretinger, R., Bruckner-Tuderman, L., and Nyström, A. (2015). High local concentrations of intradermal MSCs restore skin integrity and facilitate wound healing in dystrophic epidermolysis bullosa. Mol. Ther. *23*, 1368–1379.

22. Chen, L., Xing, Q., Zhai, Q., Tahtinen, M., Zhou, F., Chen, L., Xu, Y., Qi, S., and Zhao, F. (2017). Pre-vascularization enhances therapeutic effects of human mesenchymal stem cell sheets in full thickness skin wound repair. Theranostics *7*, 117–131.

23. Ghatak, S., Chan, Y.C., Khanna, S., Banerjee, J., Weist, J., Roy, S., and Sen, C.K. (2015). Barrier function of the repaired skin is disrupted following arrest of Dicer in keratinocytes. Mol. Ther. *23*, 1201–1210.

24. Hong, H.J., Jin, S.E., Park, J.S., Ahn, W.S., and Kim, C.K. (2008). Accelerated wound healing by smad3 antisense oligonucleotides-impregnated chitosan/alginate polyelectrolyte complex. Biomaterials *29*, 4831–4837.

25. Frauenstein, K., Sydlik, U., Tigges, J., Majora, M., Wiek, C., Hanenberg, H., Abel, J., Esser, C., Fritsche, E., Krutmann, J., and Haarmann-Stemmann, T. (2013). Evidence for a novel anti-apoptotic pathway in human keratinocytes involving the aryl hydrocarbon receptor, E2F1, and checkpoint kinase 1. Cell Death Differ. *20*, 1425–1434.

26. Shi, Y., Zhou, W., Cheng, L., Chen, C., Huang, Z., Fang, X., Wu, Q., He, Z., Xu, S., Lathia, J.D., et al. (2017). Tetraspanin CD9 stabilizes gp130 by preventing its ubiquitin-dependent lysosomal degradation to promote STAT3 activation in glioma stem cells. Cell Death Differ. *24*, 167–180.

27. Zheng, J., Liu, X., Wang, P., Xue, Y., Ma, J., Qu, C., and Liu, Y. (2016). CRNDE Promotes Malignant Progression of Glioma by Attenuating miR-384/PIWIL4/STAT3 Axis. Mol. Ther. *24*, 1199–1215.

28. Fujita, Y., Yagishita, S., Hagiwara, K., Yoshioka, Y., Kosaka, N., Takeshita, F., Fujiwara, T., Tsuta, K., Nokihara, H., Tamura, T., et al. (2015). The clinical relevance of the miR-197/CKS1B/STAT3-mediated PD-L1 network in chemoresistant non-small-cell lung cancer. Mol. Ther. *23*, 717–727.

29. Ai, X.Y., Liu, H.J., Lu, C., Liang, C.L., Sun, Y., Chen, S., Sun, B., Li, Y., Liu, Y.R., Zhang, Q., et al. (2017). Phenytoin silver: a new nanocompound for promoting dermal wound healing via comprehensive pharmacological action. Theranostics *7*, 425–435.

30. Li, H., Chang, L., Du, W.W., Gupta, S., Khorshidi, A., Sefton, M., and Yang, B.B. (2014). Anti-microRNA-378a enhances wound healing process by upregulating integrin beta-3 and vimentin. Mol. Ther. *22*, 1839–1850.

31. Deveza, L., Choi, J., Lee, J., Huang, N., Cooke, J., and Yang, F. (2016). Polymer-DNA nanoparticle-induced CXCR4 overexpression improves stem cell engraftment and tissue regeneration in a mouse hindlimb ischemia model. Theranostics *6*, 1176–1189.

32. Miura, N., Shaheen, S.M., Akita, H., Nakamura, T., and Harashima, H. (2015). A KALA-modified lipid nanoparticle containing CpG-free plasmid DNA as a potential DNA vaccine carrier for antigen presentation and as an immune-stimulative adjuvant. Nucleic Acids Res. *43*, 1317–1331.

33. Jeyapalan, Z., Deng, Z., Shatseva, T., Fang, L., He, C., and Yang, B.B. (2011). Expression of CD44 3′-untranslated region regulates endogenous microRNA functions in tumorigenesis and angiogenesis. Nucleic Acids Res. *39*, 3026–3041.

34. Yang, Q., et al. (2017). A circular RNA promotes tumorigenesis by inducing c-myc nuclear translocation. Cell Death Differ., Published online June 5, 2017. http://dx.doi.org/10.1016/j.ymthe.2017.05.022.

35. Rutnam, Z.J., Du, W.W., Yang, W., Yang, X., and Yang, B.B. (2014). The pseudogene TUSC2P promotes TUSC2 function by binding multiple microRNAs. Nat. Commun. *5*, 2914.

36. Du, W.W., Liu, F., Shan, S.W., Ma, X.C., Gupta, S., Jin, T., Spaner, D., Krylov, S.N., Zhang, Y., Ling, W., and Yang, B.B. (2015). Inhibition of dexamethasone-induced fatty liver development by reducing miR-17-5p levels. Mol. Ther. *23*, 1222–1233.

37. Li, X., Wu, Q., Bu, M., Hu, L., Du, W.W., Jiao, C., Pan, H., Sdiri, M., Wu, N., Xie, Y., and Yang, B.B. (2016). Ergosterol peroxide activates Foxo3-mediated cell death signaling by inhibiting AKT and c-Myc in human hepatocellular carcinoma cells. Oncotarget *7*, 33948–33959.

38. Du, W.W., Fang, L., Yang, W., Wu, N., Awan, F.M., Yang, Z., and Yang, B.B. (2017). Induction of tumor apoptosis through a circular RNA enhancing Foxo3 activity. Cell Death Differ. *24*, 357–370.

YMTHE, Volume *25*

Supplemental Information

The Circular RNA Interacts with STAT3, Increasing Its Nuclear Translocation and Wound Repair by Modulating Dnmt3a and miR-17 Function

Zhen-Guo Yang, Faryal Mehwish Awan, William W. Du, Yan Zeng, Juanjuan Lyu, De Wu, Shaan Gupta, Weining Yang, and Burton B. Yang

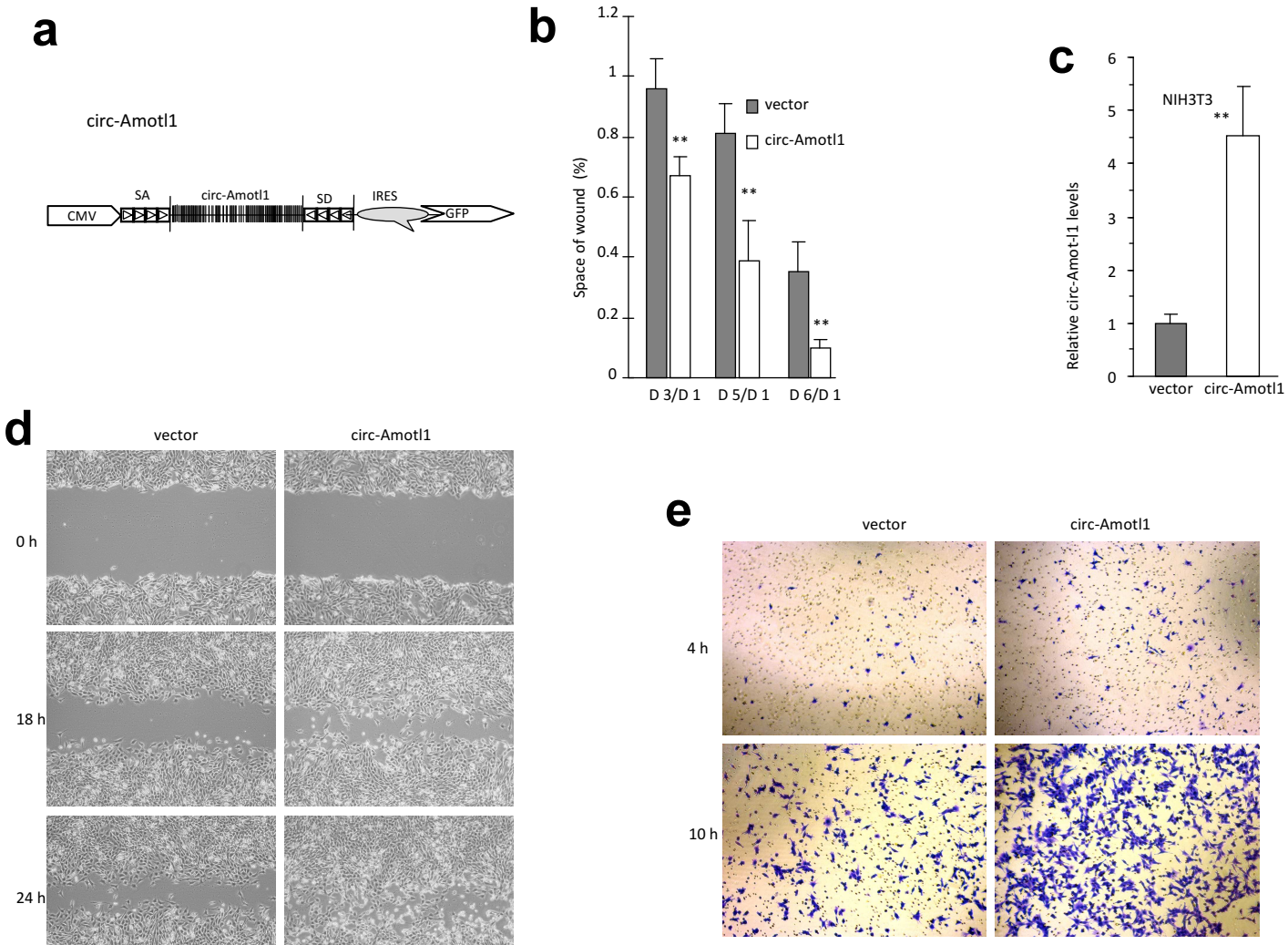

Fig S1. circ-Amotl1 enhanced wound healing and migration

(a). Structure of circ-Amotl1

(b) The ratio of wound sizes on the third, fifth and sixth days to that on the first day indicated faster wound healing process in the circ-Amotl1-injected side. ** *p<0.01,* Error bars, ±S.D, *n=10*.

(c) RNAs extracted from NIH3T3 cells transfected with circ-Amotl1 were subject to RT and real-time PCR to detect circ-Amotl1 levels. Significant increase in circ-Amotl1 levels was detected in the circ-Amotl1-transfected cells. ** *p <0.01.* Error bars, S.D (*n=4*).

(d) Upper, Scratch wound healing assay was performed to measure the motility of NIH3T3 cells transfected with circ-Amotl1 and control vector. Overexpression of circ-Amotl1 enhanced cell migration. Lower, Quantitaion of the migration. ** *p <0.01.* Error bars, S.D (*n=5*).

(e) Typical pictures of trans-well migration assay.

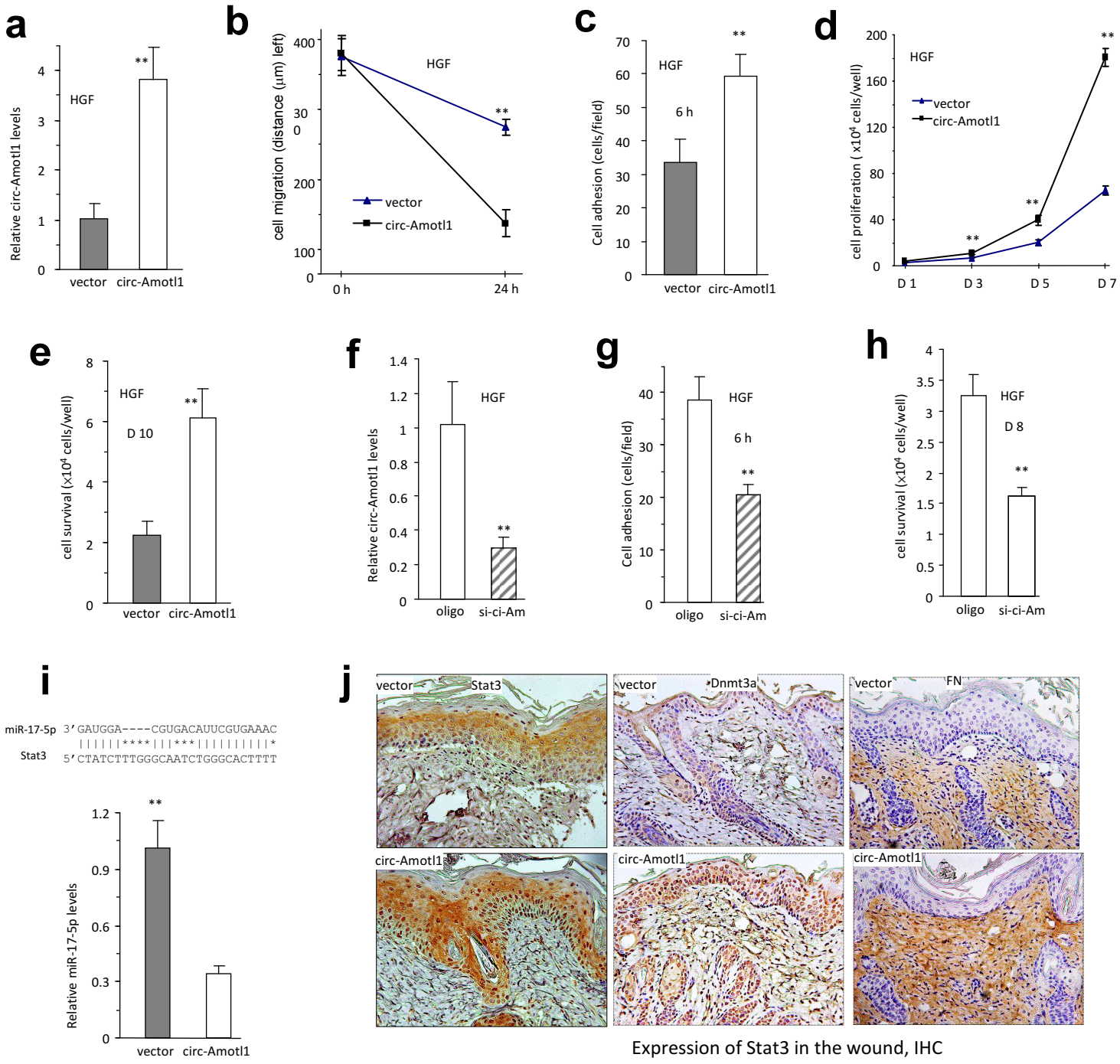

Fig S2. circ-Amotl1 enhanced cell proliferation, migration, and survival

(a) RNAs extracted from HGF cells transfected with circ-Amotl1 or control vector were subject to real-time PCR. Up-regulation of circ-Amotl1 was detected in the circ-Amotl1-transfected cells. ** *p<0.01.* Error bars, S.D (*n=4*).

(b) Wound healing assay showed that overexpression of circ-Amotl1 increased migration of the HGF cells. ** *p <0.01,* Error bars, S.D (*n=5*).

(c) Overexpression of circ-Amotl1 increased HGF cell adhesion.

(d) Cell proliferation assay showed that HGF cells transfected with circ-Amotl1 proliferated faster than the control. ** *p <0.01,* Error bars, S.D (*n=5*).

(e) Maintained in serum-free medium for 10 days, HGF cells transfected with circ-Amotl1 displayed increase in survival relative to the control. ** *p <0.01,* Error bars, S.D (*n=5*).

(f) Down-regulation of circ-Amotl1 was detected in the siRNA-transfected cells as compared to the control. ***p <0.01,* Error bars, S.D (*n=4*).

(g) Silencing circ-Amotl1 repressed cell adhesion on Petri-dish in HGF cells after 6 h incubation. ** *p <0.01,* Error bars, S.D (*n=5*)

(h) Silencing circ-Amotl1 repressed HGF cell survival after being maintained in serum-free medium for 8 days. ** *p <0.01,* Error bars, S.D (*n=5*).

(i) Ectopic expression of circ-Amotl1 decreased miR-17-5p expression.

(j) Sections of wound tissues from circ-Amotl1- and control plasmid-injected mice were subject to immunohistochemistry staining. Increased expression of Stat3, Dnmt3a, and fibronectin was detected in circ-Amotl1-injected mice.

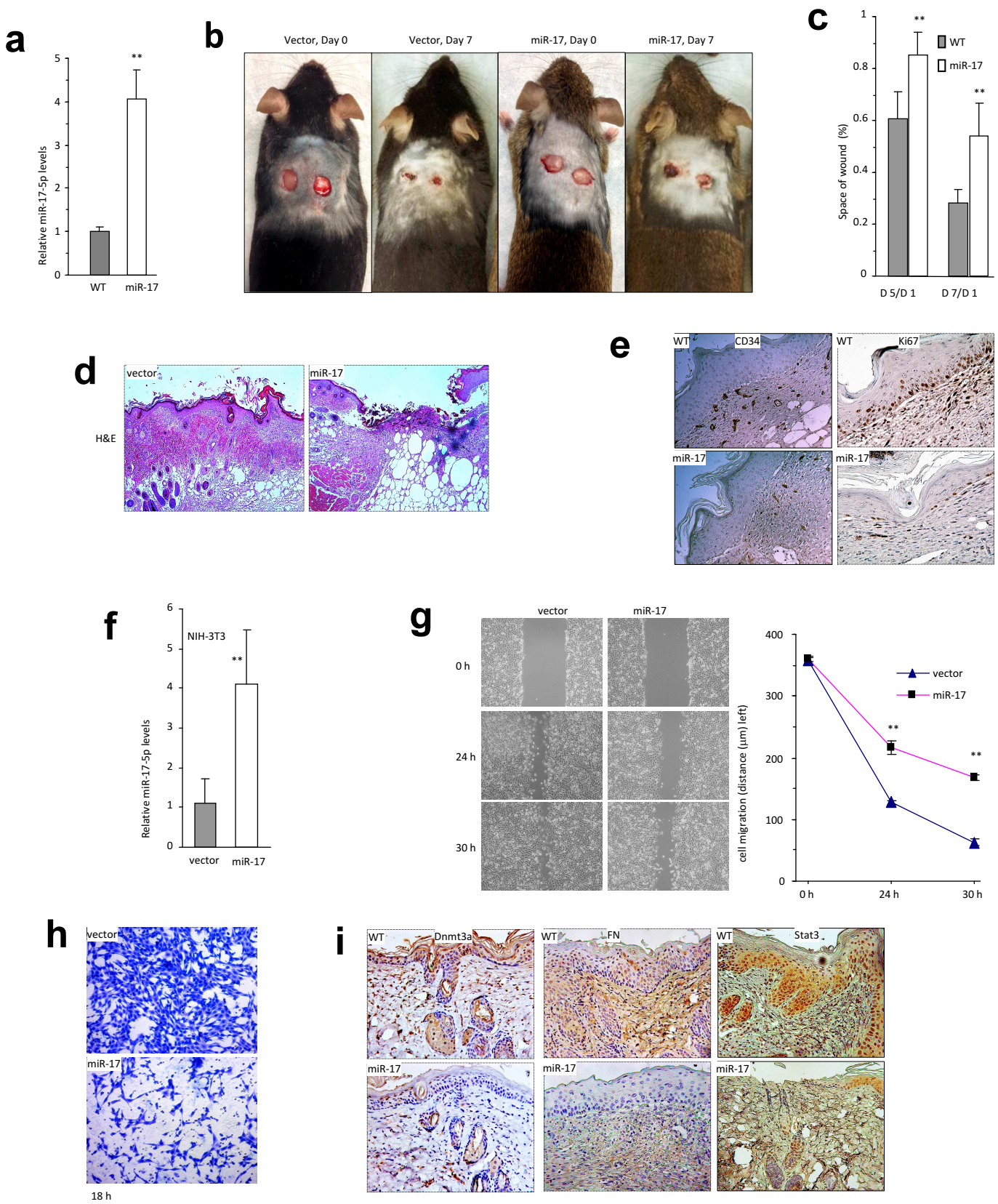

Fig S3. Mutual regulation of circ-Amotl1 and miR-17-5p. **(a)** Wound tissues were subject to real-time PCR to confirm up-regulation of miR-17-5p. **(b)** Typical pictures were taken from seventh day showing that miR-17 transgenic mice had delayed healing compared to the wild-type group. **(c)** After mice were slaughtered, wound size was measured by multiplying longest length by greatest width. The ratio of wound sizes on the fifth and seventh day to that on the first day indicated slower wound healing process in the miR-17 transgenic mice relative to controls. **(d)** Typical pictures of H&E staining showing larger wound in the miR-17 tissue. **(e)** Immunohistochemistry staining of wound tissues showed decreased levels of CD34 (left) and Ki67 (right). **(f)** Cell lines stably transfected with miR-17 or the control vector were subject to real-time PCR to confirm up-regulation of miR-17-5p. **(g)** Left, scratch wound healing assay was performed to measure the motility of NIH3T3 cells transfected with miR-17 and control vector. Overexpression of miR-17 decreased cell migration. Right, Quantitaion of the migration. ** $p < 0.01$. Error bars, S.D ($n=5$). **(h)** Typical picture of trans-well migration assay. **(i)** Typical pictures of immunohistochemistry staining showed decreased expression of Dnmt3a, fibronectin, and Stat3 in the miR-17 transgenic mice.

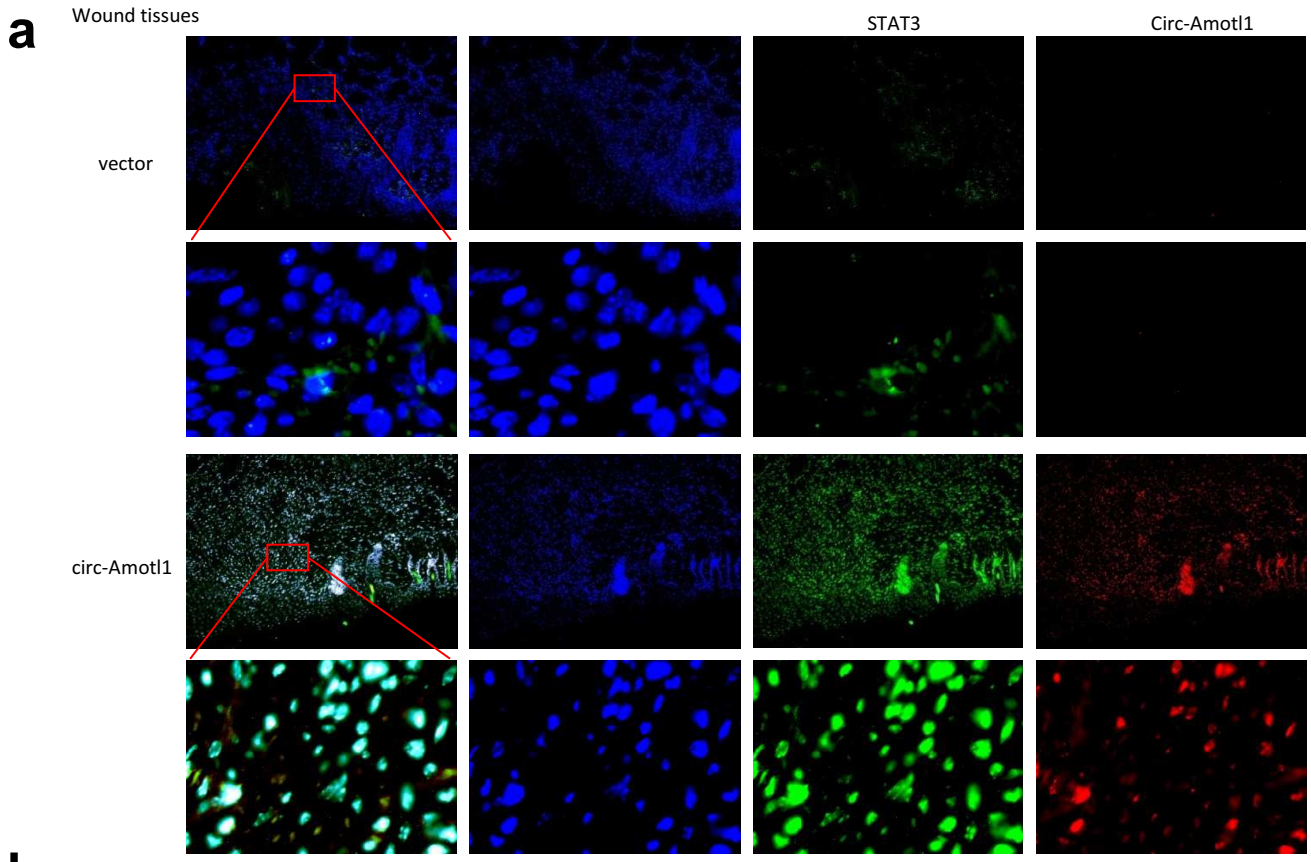

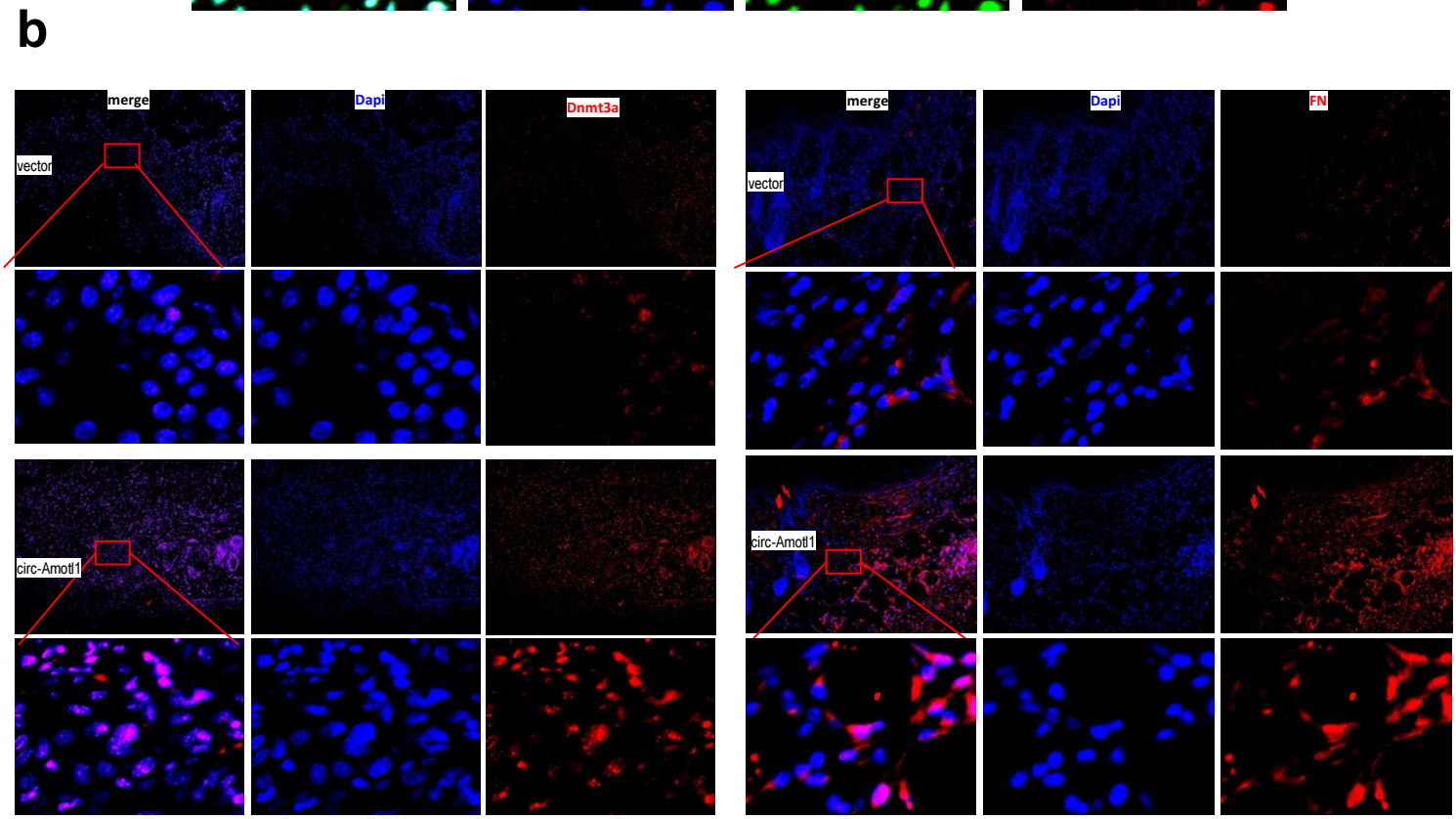

Fig S4. Delivery of circ-Amotl1 in wound tissues increased expression of Stat3, Dnmt3a and fibronectin

(a) The mock- and circ-Amotl1-injected tissues were stained with DAPI (blue), Stat3 (green), and circ-Amotl1 (red). High intensity of Stat3 and circ-Amotl1 were detected in the nuclei.

(b) The mock- and circ-Amotl1-transfected injected tissues were stained with DAPI and Dnmt3a (red, left) or fibronectin (red, right). High intensity of Stat3 and fibronectin were detected in the circ-Amotl1-injected tissues.

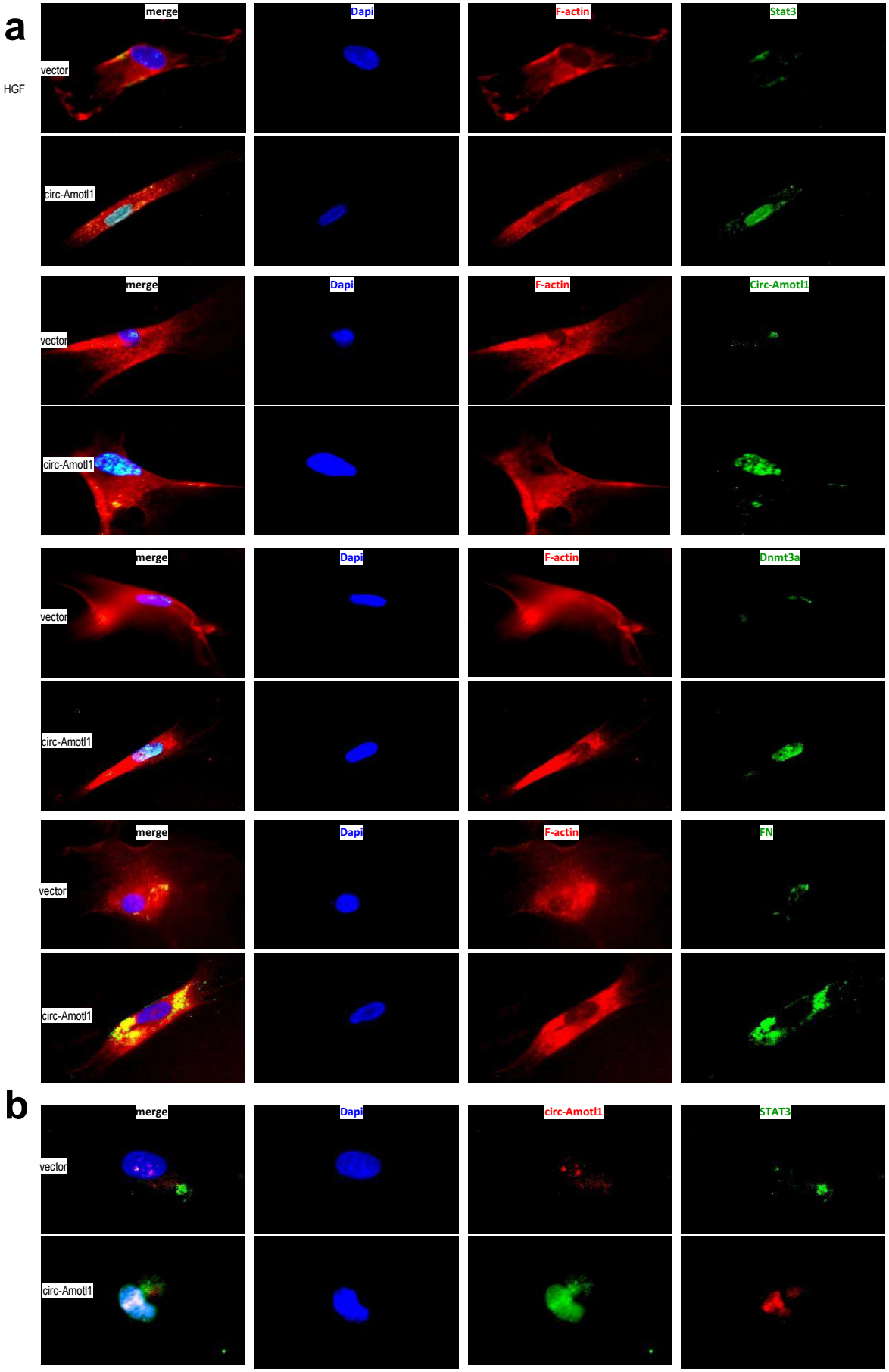

Fig S5. Expression of circ-Amotl1 in HGF cells increased expression of Stat3, Dnmt3a and fibronectin. (a) The mock- and circ-Amotl1-transfected HGF cells were stained with DAPI (blue), F-actin (red) and Stat3, Dnmt3a, fibronectin, or in situ hybridized with circ-Amotl1 (green). Increased expression of these molecules was detected in the circ-Amotl1-transfected cells. (b) The cells were stained with DAPI (blue), circ-Amotl1 (green), and Stat3 (red). Co-localization of circ-Amotl1 and Stat3 was detected in the circ-Amotl1-transfected cells.

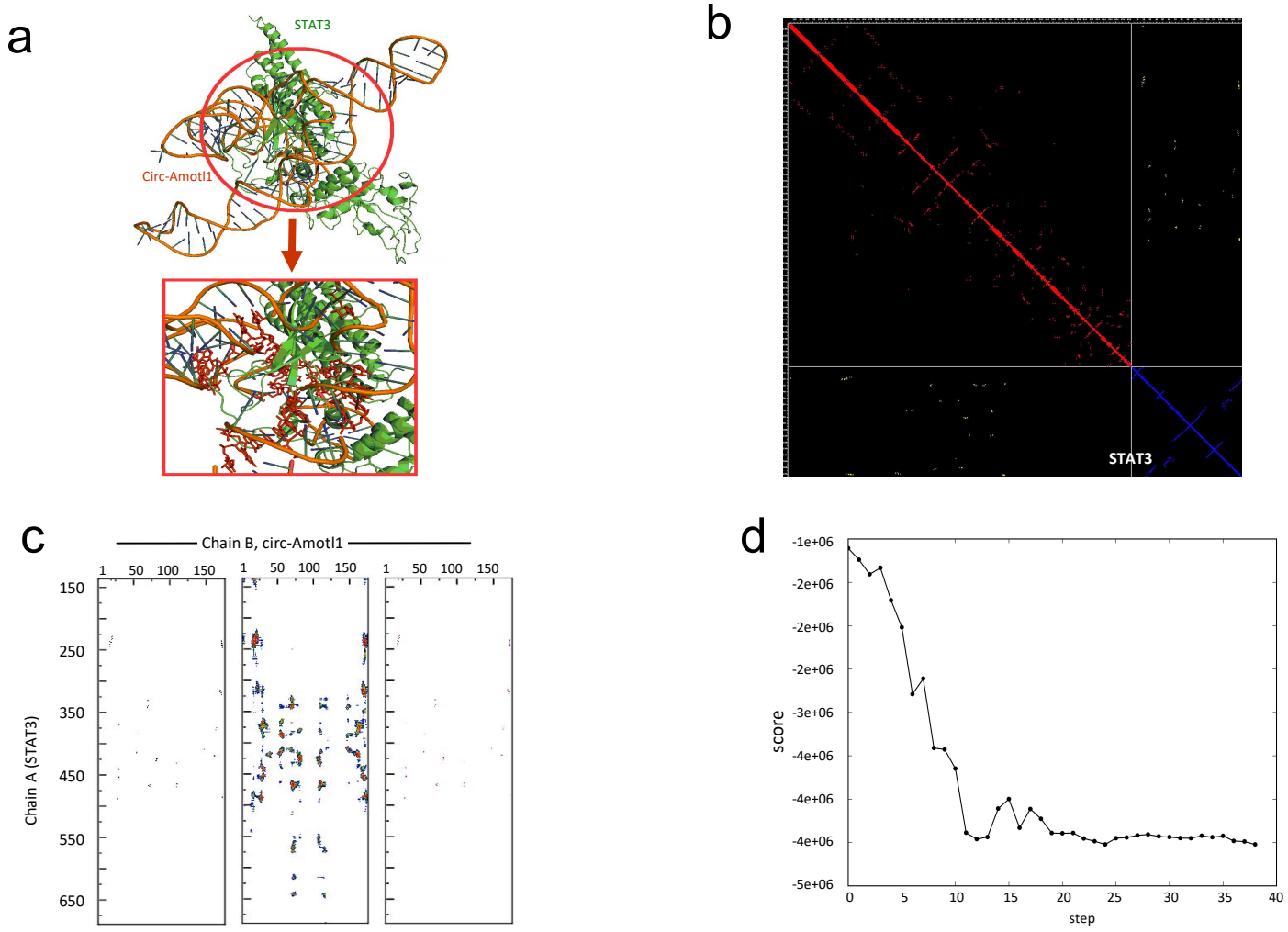

e

name	sequence
27.38.hu.Cir.Amotl1-R	5′ ggtt ggggt gcc ata ccgc ag ttg
27.39.hu.Cir.Amotl1-F	5′ cagcctgtgagaacagatgtggcc
28.76.hu.Amotl1-F	5′ cgcctcatgtggagggcaaagttg
28.77.hu.Amotl1-R	5′ ccct gatg ctac tggttg cctcca
27-77.musDnmt3a-SacI	5′ ccc gagctc gggctgggatcagtggccaatagg
27-78.musDnmt3a-MluI	5′ cc acgcgt acc ttg tcaaa gaaaaag caa gaa
26.27mus.Stat3-F	5′ ccgacccaggtagtgctgc
26.28.mus.Stat3-R	5′ caatggtattgctgcaggtcg
25-66.musFN1-F	5′ gaagacagatgagcttcccca
25-67.musFN1-R	5′ ggttggtgatgaaggggtc
21-60.hsa-miR-17-5p	5′caaagtgcttacagtgcag
circ-Amotl1 probe	5′ caaagaggatcttcaactcgttaccccatact
Blocking oligo	5'cggaacctctcatttccacctctgagatcctcaggaagtttgggg agtggaagttacaaagaggatcttcaactcgttaccccatact
control oligo	5' tccttcctctctttctctcccttgtga
siRNA	5′ GGGGUAACGAGUUGAAGAUUU 5′ AUCUUCAACUCGUUACCCCUU

Fig S6. Computational analysis of circ-Amotl1 interacting with Stat3

(a) Graphic three-dimensional structures of the docking models of circ-Amotl1 with Stat3.
(b) The contact map in the binding residues between circ-Amotl1 and Stat3.
(c) The residue-level resolution contact maps in the binding residues between circ-Amotl1 and Stat3.
(d) Refinement of the best docked circ-Amotl1-Stat3 model showing MC score vs. steps of simulation.
(e) Primer sequences used for the study.

Table S1. The circ-Amotl1-STAT3 Distance

N(res No)	atom	chain	AA (res No)	atom	chain	distance	type
LYS 140	NZ	A	A 18	O3′	B	2.3	Phil phil
LYS 140	NZ	A	A 19	OP1	B	2.75	Phil phil
GLU 229	O	A	U 21	OP1	B	3.47	Phil phil
TYR 230	O	A	C 20	OP2	B	1.69	Phil phil
TYR 230	OH	A	A 19	O2′	B	2.02	Phil phil
LYS 233	CD	A	C 20	O3′	B	2.37	Phil phil
LYS 233	CE	A	U 21	OP2	B	0.33	Phil phil
THR 234	N	A	C 20	OP2	B	2.44	Phil phil
THR 234	OG1	A	A 19	O3′	B	2.6	Phil phil
THR 236	O	A	A 170	O4′	B	1.47	Phil phil
ASP 237	OD1	A	A 170	OP1	B	2.74	Phil phil
ASP 237	O	A	U 17	OP2	B	2.43	Phil phil
GLU 238	OE1	A	A 18	O3′	B	2.83	Phil phil
GLU 238	OE2	A	C 20	OP1	B	3.1	Phil phil
GLU 238	OE1	A	A 19	C5′	B	0.84	Phil phil
LEU 240	O	A	A 170	N3	B	1.51	Phob phil
ALA 241	CB	A	A 170	O2′	B	1.58	Phob phil
ALA 241	O	A	A 171	O4′	B	3.42	Phob phil
ASP 242	OD1	A	U 17	C2	B	1.39	Phil phil
TRP 243	CE3	A	A 170	N1	B	1.95	Phil phil
TRP 243	CZ3	A	A 171	N1	B	2.86	Phil phil
LYS 244	CB	A	A 171	C4	B	1.42	Phil phil
LYS 244	CG	A	A 170	C2	B	1.68	Phil phil
ARG 245	CB	A	U 17	C5	B	3.28	Phil phil
ARG 245	N	A	A 171	N3	B	3.3	Phil phil
GLN 247	OE1	A	A 171	N1	B	2.76	Phil phil
GLN 248	OE1	A	A 171	O2′	B	3	Phil phil
ASN 315	OD1	A	G 168	O3′	B	2.57	Phil phil
ASN 315	OD1	A	U 169	OP1	B	1.96	Phil phil
LYS 318	NZ	A	G 168	C4′	B	2.08	Phil phil
SER 319	OG	A	U 169	O3′	B	3.41	Phil phil
SER 319	OG	A	A 170	OP1	B	3.48	Phil phil
VAL 322	CG1	A	A 170	N6	B	3.39	Phob phil
MET 331	SD	A	U 69	O2′	B	2.52	Phob phil
HIS 332	CE1	A	C 70	C5′	B	2.74	Phil phil
HIS 332	NE2	A	U 69	O3′	B	2.96	Phil phil
LYS 340	NZ	A	C 70	OP2	B	2.41	Phil phil
GLY 342	O	A	U 69	OP1	B	2.84	Phob phil
VAL 343	CG2	A	U 69	OP1	B	1.97	Phob phil
LYS 370	CE	A	C 30	OP2	B	1.5	Phil phil
LYS 370	CB	A	C 29	OP1	B	3.01	Phil phil
ASP 371	OD2	A	C 30	N4	B	3.41	Phil phil
SER 372	OG	A	C 28	OP2	B	2.57	Phil phil
VAL 373	O	A	A 163	OP2	B	2.61	Phob phil
ARG 379	NH1	A	U 162	OP1	B	3.08	Phil phil
ASN 385	OD1	A	G 54	OP1	B	3	Phil phil

Table S1. The circ-Amotl1-STAT3 Distance (con.)

N(res No)	atom	chain	AA (res No)	atom	chain	distance	type
ASN 385	CB	A	U 55	OP1	B	3.19	Phil phil
LEU 387	CD2	A	U 55	OP2	B	3.37	Phob phil
HIS 410	ND1	A	C 146	O2′	B	2.84	Phil phil
ARG 414	NH1	A	G 54	OP2	B	2.78	Phil phil
GLU 415	O	A	G 54	OP1	B	3.45	Phil phil
GLN 416	CD	A	A 160	OP1	B	2.69	Phil phil
GLY 419	CA	A	A 160	O2′	B	2.45	Phob phil
ASN 420	N	A	A 160	O2′	B	2.73	Phil phil
ASN 420	ND2	A	G 161	C4′	B	0.4	Phil phil
ARG 423	NH1	A	G 80	C4′	B	1.61	Phil phil
ARG 423	O	A	G 81	C5′	B	2.04	Phil phil
ASN 425	O	A	G 81	C4′	B	2.35	Phil phil
ASN 425	N	A	C82	OP1	B	3.44	Phil phil
CYS 426	CA	A	G 81	O2′	B	3.07	Phil phil
ALA 428	CB	A	G 80	O2′	B	3.22	Phob phil
ALA 428	N	A	G 81	O4′	B	3.15	Phob phil
ILE 431	CG2	A	G 107	O2′	B	2.73	Phob phil
VAL 432	CG1	A	U 109	OP2	B	3.35	Phob phil
VAL 432	CG2	A	A 108	O3′	B	2.92	Phob phil
LEU 438	CD1	A	C 28	C5′	B	1.69	Phob phil
THR 440	OG1	A	C 28	O3′	B	2.48	Phil phil
THR 440	CG2	A	C 29	C5′	B	1.57	Phil phil
GLU 442	OE1	A	C 30	OP1	B	0.43	Phil phil
GLU 442	CD	A	C 29	O3′	B	1.94	Phil phil
ASP 453	OD2	A	C 30	O2′	B	3.05	Phil phil
GLU 455	OE1	A	C 30	C6	B	3.26	Phil phil
GLU 455	OE2	A	C 29	O4′	B	0.48	Phil phil
HIS 457	ND1	A	C 28	O2′	B	2.38	Phil phil
SER 465	OG	A	C 110	OP1	B	2.94	Phil phil
SER 465	OG	A	U 109	OP2	B	3.13	Phil phil
ASN 466	ND2	A	G 72	O6	B	2.63	Phil phil
ILE 467	CG2	A	C 71	OP2	B	0.47	Phob phil
ILE 467	CD1	A	C 70	OP1	B	1.8	Phob phil
CYS 468	CB	A	G 72	OP2	B	3.04	Phil phil
CYS 468	N	A	C 71	OP2	B	3	Phil phil
GLN 469	NE2	A	U 109	OP1	B	1.31	Phil phil
GLN 469	NE2	A	A 108	O3′	B	3.23	Phil phil
ASN 485	O	A	C 172	P	B	2.4	Phil phil
ASN 485	O	A	A 171	O3′	B	1.63	Phil phil
ASN 486	CA	A	C 172	OP2	B	1.18	Phil phil
ASN 486	CA	A	A 171	O3′	B	3.23	Phil phil
PRO 487	N	A	C 172	OP1	B	1.05	Phob phil
PRO 487	CD	A	A 171	O3′	B	2.44	Phob phil
LYS 488	CD	A	C 28	O4′	B	3.04	Phob phil
LYS 488	NZ	A	U 27	C2	B	0.49	Phil phil
LYS 488	NZ	A	C 172	O2′	B	3.18	Phil phil
ASN 489	N	A	U 27	O2′	B	3.26	Phil phil

The table reporting a list of atoms “in contact” (within the distance cutoff) with relative distances less than 3.5Å.

Table S2. Accessible Surface Area table of circ-Amolt1-Stat3 complex

Buried area upon the complex formation (A^2) 6316.2
Buried area upon the complex formation (%) 11.13
Interface area (A^2) 3158.1
Interface area STAT3 (%) 11.77
Interface area circ-AMOTL1 (%) 10.56
POLAR Buried area upon the complex formation (A^2) 2667.0
POLAR Interface (%) 42.22
POLAR Interface area (A^2) 1333.5
NON POLAR Buried area upon the complex formation (A^2) 3649.2
NON POLAR Interface (%) 57.78
NON POLAR Interface area (A^2) 1824.6
Residues at the interface_total (n) 148
Residues at the interface_STAT3 96
Residues at the interface_circ-AMOTL1 52

Table S3. circ-Amolt1-Stat3 interaction overview

Number of interacting residues STAT3 **60**
Number of interacting residues circ-AMOTL1 **32**
Number of hydrophilic-hydrophobic interaction **20**
Number of hydrophilic-hydrophilic interaction **73**
Number of hydrophobic-hydrophobic interaction **0**